# Development of the Surface Urban Energy and Water balance Scheme (SUEWS) for cold climate cities

L. Järvi[1], C. S. B. Grimmond[2], M. Taka[3], A. Nordbo[1], H. Setälä[4] and I. B. Strachan[5]

[1]{University of Helsinki, Department of Physics, Helsinki, Finland}

[2]{University of Reading, Department of Meteorology, Reading, United Kingdom}

[3]{University of Helsinki, Department of Geosciences and Geography, Helsinki, Finland}

[4]{University of Helsinki, Department of Environmental Sciences, Helsinki, Finland}

[5]{McGill University, Department of Natural Resource Sciences, QC, Canada}

Correspondence to: L. Järvi (leena.jarvi@helsinki.fi)

**Abstract**

The Surface Urban Energy and Water balance Scheme (SUEWS) is developed to include snow. The processes addressed include accumulation of snow on the different urban surface types; snow albedo and density aging, snow melting and re-freezing of melt water. Individual model parameters are assessed and independently evaluated using long-term observations in the two cold climate cities of Helsinki and Montreal. Eddy covariance sensible and latent heat fluxes and snow depth observations are available for two sites in Montreal and one in Helsinki. Surface runoff from two catchments (24 and 45 ha) in Helsinki and snow properties (albedo and density) from two sites in Montreal are also analysed. As multiple observation sites with different land-cover characteristics are available in both cities, model development is conducted independently of evaluation.

The developed model simulates snowmelt related runoff well (within 19% and 3% for the two catchments in Helsinki when there is snow on the ground), with the springtime peak estimated correctly. However, the observed runoff peaks tend to be smoother than the simulated ones, likely due to the water holding capacity of the catchments and the missing time lag between the catchment and the observation point in the model. For all three sites the model simulates the timing of the snow accumulation and melt events well, but underestimates the total snow depth by 18-20% in Helsinki and 29-33% in Montreal. The

1   model is able to reproduce the diurnal pattern of net radiation and turbulent fluxes of sensible

2   and latent heat during cold snow, melting snow and snow-free periods. Largest model

3   uncertainties are related to the timing of the melting period and the parameterization of the

4   snow melt. The results show that the enhanced model can simulate correctly the exchange of

5   energy and water in cold climate cities at sites with varying surface cover.

6

## 7   1   Introduction

8   Today more than half of world's population resides in urban areas, and this fraction is

9   expected to increase in the next decades (Martine and Marshall, 2007). Thus, the ability to

10   understand and forecast the urban climate is crucial for sustainable urban planning and our

11   quality of life. The exchanges of heat and water between the surface and the atmosphere are

12   of great importance to urban climate studies. These exchanges describe the surface forcing in

13   numerical weather prediction, air quality and climate models.

14   In urban areas several land surface models, with different complexity, simulate these energy

15   exchanges, but none of the models consistently outperforms the others (Grimmond et al.,

16   2011). The latent heat flux is commonly underestimated and sometimes even ignored, which

17   further increases the direct heat emissions to the atmosphere. Furthermore, most of these

18   models only concentrate on the surface-atmosphere interactions without any connections to

19   the water cycles in urban areas. Similarly, several hydrological models to simulate urban

20   drainage and the surface runoff in urban areas have been developed (Mitchell et al., 2003,

21   2008; Easton et al., 2007; Jacobson, 2011), but these do not typically consider the full energy

22   balance.

23   Both in land surface and hydrological model studies, urban areas located in cold climates

24   have been little studied despite their particular sensitivity to regional and global climate

25   change. Thus appropriate, robust, well tested modeling tools are needed. Modeling studies of

26   cold cities are focused on a few sites mainly in North-America (e.g. Valeo and Ho, 2004;

27   Lemonsu et al., 2010; Leroyer et al., 2010) and Scandinavia (e.g. Semádeni-Davies et al.,

28   1998). These emphasize the need for correct description of snow cover in hydrological

29   models. Snow affects surface energy partitioning via albedo and snowmelt, re-freezing and

30   the phase change related energy fluxes. The energy required for snow melt can be of the same

31   magnitude as the sensible and latent heat fluxes (Lemonsu et al., 2010). Snow impacts water

32   availability and its melt may cause springtime floods in urban areas (Semádeni-Davies and

1 Bengtsson, 1998). To keep cities operational, snow is often redistributed within

2 neighborhoods and/or is transported away (Semádeni-Davies and Bengtsson, 1998, 1999),

3 which impacts both the energy and water cycles.

4 The lack of observational data in urban areas with continuous winter snow cover makes the

5 determination of model parameters and flux evaluation challenging. Surface-atmosphere

6 exchange of sensible and latent heat can be measured directly using the eddy covariance

7 technique, but these observations are relatively rare especially in cold climate cities. Notable

8 exceptions include the work of Lemonsu et al. (2008), Vesala et al. (2008), Bergeron and

9 Strachan (2012) and Nordbo et al. (2012a,b). These studies have found a strong seasonality in

10 the energy exchanges and a need for correct estimation of anthropogenic heat emissions from

11 building sources, notably heating in winter. Similarly, the few hydrological studies have

12 shown strong seasonality in stormwater runoff and differences in the amount of the snow

13 melt when compared to natural environments (Bengtsson and Westerström, 1992; Semádeni-

14 Davies and Bengtsson, 1998; Valtanen et al., 2013).

15 The purpose of this study is to develop a model that can correctly simulate both the energy

16 and water balances in cold climate cities. The model developed is included in the Surface

17 Urban Energy and Water balance Scheme (SUEWS, Järvi et al., 2011) with particular

18 attention to the accumulation and melting of snow. The development and independent

19 evaluation of the model uses several years of data collected in Helsinki (60°N, 24°W) and

20 Montreal (45°N, 73°W). These include turbulent fluxes of heat and water measured with the

21 eddy covariance technique, stormwater runoff and snow properties. In addition to snow

22 related processes, the parameterization of the leaf area index has been improved to be more

23 applicable for cold climate cities (Appendix A).

24

25 **2   Methods**

26 **2.1 The Surface Urban Energy and Water balance Scheme (SUEWS)**

27 The Surface Urban Energy and Water balance Scheme SUEWS (Järvi et al., 2011) simulates

28 the urban energy and water balance components from local or neighborhood scale using

29 hourly meteorological forcing data. These data inputs are kept to a minimum to enhance the

30 flexibility of the model and commonly include: measured solar radiation (probably least

31 frequently measured), air temperature, relative humidity, surface air pressure, wind speed and

1 precipitation. In addition, SUEWS requires information about the characteristics of the area

2 to be simulated, such as surface cover fractions of paved, buildings, evergreen trees/shrubs,

3 deciduous trees/shrubs, irrigated grass, non-irrigated grass and water, and population density

4 and building and tree heights.

5 Rates of evaporation-interception for a single layer for each of the surface types are

6 calculated and below each surface type, except water, there is a single soil layer. At each time

7 step (5 min to 1 h) the moisture state of each surface and soil type is calculated. Horizontal

8 water movements at the surface and in the soil are incorporated. Latent heat flux is calculated

9 with a modified Penman-Monteith equation and sensible heat flux as a residual from the

10 available energy minus the latent heat. The model contains several sub-models, for example

11 for net all-wave radiation (NARP, Offerle et al., 2003; Loridan et al., 2011), storage heat

12 fluxes (Grimmond et al., 1991), anthropogenic heat fluxes, and external irrigation.

13 **2.1.1 New developments**

14 The new version of SUEWS presented here incorporates a parameterization for snow cover.

15 Previously, snow cover was a required input that was assumed to cover the whole grid area

16 and only directly impacted the radiation. Now, accumulation and melting of snow are

17 estimated, with impact to net all-wave radiation, evaporation, and other water balance

18 components included. For each surface type, the energy and water balances are calculated

19 separately for snow-free and snow-covered areas and the model outputs are weighted

20 according to their respective fractions. The energy and water flow calculations in the snow-

21 free surface types follow those in the original version of the model (Järvi et al., 2011). Here

22 we present the equations related to the snow covered surface which is treated as a single snow

23 layer.

24 The energy balance of the snow covered surface modified for urban areas can be written as

25 (e.g. Oke, 1987; Cline, 1997)

26 $$Q_M + \Delta Q_{S,I} = Q^* + Q_F - Q_H - Q_E + Q_P - Q_g + \Delta Q_A \quad \text{(W m}^{-2}\text{)} \qquad (1)$$

27 where $Q_M$ is the latent heat storage change caused by melting or freezing, $\Delta Q_{s,I}$ is the change

28 in the storage heat of the snow, $Q^*$ is the net all-wave radiation, $Q_F$ is the anthropogenic heat

29 flux, $Q_H$ and $Q_E$ are the turbulent sensible and latent heat fluxes, $Q_P$ is the heat released by

30 liquid precipitation on snow, $Q_g$ is the heat exchange between the snow and the soil below

31 and $\Delta Q_A$ is the net advective heat flux. Snow melt occurs if the net energy input to the snow is

1   positive (i.e. right-hand side of the eq. (1) > 0). $Q_F$ is calculated based on cooling and heating

2   degree days (Järvi et al., 2011). Advection occurs at a number of scales. The micro-scale (or

3   sub-grid-scale) advection is not resolved in the model, but rather embedded within the

4   coefficients obtained using model optimization. The inter-grid advection is assumed to be

5   negligible. This is consistent with the eddy covariance fluxes used to assess the model.  To

6   resolve advection at this scale would require the model to be embedded in a meso-scale

7   model. The ground heat flux $Q_g$ is not separately resolved and is assumed to be  included

8   within the parameterization coefficients.

9   The link to the snow mass balance is through $Q_E$ or evaporation ($E$):

10   $$P + F = E + R + T_R + \Delta S_{WE} \quad \text{(mm h}^{-1}\text{)} \tag{2}$$

11   where $P$ is precipitation (snowfall, rain), $F$ is liquid water that freezes on a snow-free surface,

12   $R$ is the runoff from the snowpack, $T_R$ is the transport of snow from the study area (e.g. via

13   snow-clearing) and $\Delta S_{WE}$ is the change in (liquid and solid phase) snow water equivalent

14   ($S_{WE}$).

15   *Surface albedo*

16   Snow affects $Q^*$ by modifying the albedo of the surface and thus the reflected short-wave

17   radiation, and the upwelling long wave radiation as the surface temperature of snow and

18   snow-free surface are different. The snow albedo ($\alpha_s$) varies with snow age for each time step

19   ($\Delta t$), based on whether it is the 'cold snow period' when melting does not occur (Baker et al.,

20   1990):

21   $$\alpha_s(t + \Delta t) = \alpha_s(t) - \tau_a \frac{\Delta t}{\tau_d} \tag{3}$$

22   or the 'warm snow period' when snow melt occurs (Verseghy, 1991):

23   $$\alpha_s(t + \Delta t) = \left[\alpha_s(t) - \alpha_s^{min}\right] exp\left(-\tau_f \frac{\Delta t}{\tau_d}\right) + \alpha_s^{min} \tag{4}$$

24   For simplicity, the warm snow period is defined as times when air temperature ($T_a$) is above

25   0°C. $\alpha_s^{min}$ is the minimum snow albedo, $\tau_d$ is a period of one day (86400 s), and $\tau_a$ and $\tau_f$ are

26   time constants related to the snow aging. After new snowfall, when $S_{WE}$ exceeds 2 mm

27   (Koivusalo and Kokkonen, 2002), the snow albedo is reset to its maximum (fresh snow)

28   value ($\alpha_s^{max}$). The upward long-wave radiation uses a constant snow emissivity.

29   *Snow heat storage*

1    The net heat storage in the snow can be considered to describe the convergence or divergence

2    of sensible heat fluxes within the snowpack volume. This is calculated using the objective

3    hysteresis model (OHM; Grimmond et al., 1991):

4    $$\Delta Q_{s,I} = a_1 Q^* + a_2 \frac{\Delta Q^*}{\Delta t} + a_3 \qquad\qquad (5)$$

5    where $a_1$, $a_2$ and $a_3$ parameters are set by the model user. The first term describes the direct

6    heating by radiation, the second term the hysteresis of the warming and cooling phases, and

7    the third the time lag. $\Delta Q_{s,I}$ is negative when the snowpack loses energy and the snowpack

8    cools increasing the 'cold content' of the snow (energy needed to heat the snow to 0°C), and

9    positive when the snow is heated towards 0°C and the cold content is filled. Cold content is

10   the total energy needed before the melting of snow can start (Bengtsson, 1982).

11   *Energy for melting and freezing*

12   There are two main approaches to estimate the snowmelt and refreezing of the melt water (*M*)

13   and the related energy (e.g. Martinec, 1989; Tobin et al., 2013): 1) the energy balance

14   method, where *M* is calculated as a residual from the other energy balance components, and

15   2) the degree day method where *M* is calculated using daily or hourly air temperatures and

16   possibly solar radiation. Although the first is more physically-based it requires more input

17   variables, whereas the latter uses more readily available variables. Comparisons of the two

18   methods have found insignificant differences in the melted water calculated (Kustas et al.,

19   1994; Debele et al., 2010). However, the site specific degree day parameters need to be

20   assessed (Bentsson, 1984).

21   In SUEWS the second approach is used via a radiation-temperature index for each surface

22   type *i* (Kustas et al., 1994; Semadeni-Davies et al., 2001; Tobin et al., 2013). Snowmelt

23   induced runoff is delayed by re-freezing of melted water (Bentsson, 1982), particularly in

24   spring, when the diurnal variations in air and snow surface temperatures are large. Daytime

25   melt-water refreezes after sunset, releasing energy. Traditionally, the degree-day methods

26   have utilized a daily time step, but in urban areas this has poor performance (Bengtsson,

27   1984). Therefore an hourly time step is utilized here. Melting and freezing occurs as a

28   function of air temperature ($T_a$) and $Q^*$ under three conditions:

29   $$\begin{cases} M_i = a_r Q^* & Q^* > 0 \text{ W m}^{-2}, T_a \geq 0°C \\ M_i = a_t T_a & Q^* < 0 \text{ W m}^{-2}, T_a \geq 0°C \\ M_i = a_f T_a & T_a < 0°C \end{cases} \qquad (6)$$

1 with factors for radiation melt $a_r$ (mm W$^{-1}$ h$^{-1}$), temperature melt $a_t$ and freezing $a_f$ (mm °C$^{-1}$

2 h$^{-1}$) which are typically linearly related with $a_f \leq a_t$ (Tobin et al., 2013). $M_i$ cannot be larger

3 than the amount of solid snow in the pack and the amount of freezing water cannot exceed

4 the amount of liquid water in the snow. The energy consumed in melting and re-freezing is

5 $$Q_{M,i} = \rho_w M_i L_f, \qquad\qquad (7)$$

6 where $\rho_w$ is the liquid water density at 0°C (kg m$^{-3}$) and $L_f$ is the latent heat of fusion at 0°C (J

7 kg$^{-1}$).

8 Besides re-freezing of melted water, the snowmelt runoff from the snowpack is delayed by

9 the amount of liquid water the snow can hold (Bengtsson, 1982; Semádeni-Davies and

10 Bentsson, 1998). In SUEWS, this liquid water retention capacity ($C^R$) is calculated as a

11 function of snow density ($\rho_s$, kg m$^{-3}$) (Anderson, 1979; Jin et al., 1999):

12 $$C_i^R = \begin{cases} C_{min}^R, & \rho_s \geq \rho_e \\ C_{min}^R + (C_{max}^R - C_{min}^R)\frac{\rho_s - \rho_e}{\rho_s}, & \rho_s < \rho_e \end{cases} \qquad \text{(kg kg}^{-1}\text{)} \qquad (8)$$

13 where $C_{min}^R$ and $C_{max}^R$ are the minimum and maximum capacities and $\rho_e$ is a threshold density

14 set to 200 kg m$^{-3}$. With time, the snow density changes (Verseghy, 1991):

15 $$\rho_s(t + \Delta t) = [\rho_s(t) - \rho_s^{max}]exp\left(-\frac{\tau_r \Delta t}{\tau_h}\right) + \rho_s^{max} \qquad\qquad (9)$$

16 to a maximum snow density $\rho_s^{max}$ with a time constant $\tau_r$. $\tau_h$ is the seconds in an hour (3600 s

17 h$^{-1}$). After snowfall, $\rho_s$ is calculated as the weighted average of the fresh ($\rho_s^{min}$) and previous

18 snow densities.

19 *Heat release by rain on snow*

20 A rain on snow event provides heat, when the precipitation temperature is above the

21 liquid/solid threshold ($T_{lim}$) (Sun et al., 1999):

22 $$Q_{P,i} = \rho_w c_w P_i (T_a - T_{lim}), \qquad\qquad (10)$$

23 where $c_w$ is the specific heat capacity of water (J kg$^{-1}$ K$^{-1}$), and $P_i$ is the precipitation on $i$th

24 surface (in m s$^{-1}$). Here, it is assumed that the temperature of the precipitation is at the air

25 temperature (Sun et al., 1999). Rain stays as a liquid and is routed to melt water store.

26 *Latent heat flux and evaporation*

1    To calculate the latent heat flux ($Q_E$) a modified Penman-Monteith equation is used with a

2    negligible surface resistance for the snow covered surfaces and an available energy that is

3    constrained by snowmelt and re-freezing of the melt water:

4    $$Q_{E,i} = \frac{s(Q_p - Q_S) + \frac{c_p \rho V}{r_a}}{s + \gamma},$$    (11)

5    where $s$ is the slope of the saturation vapour pressure curve over ice (Pa °C$^{-1}$) calculated

6    according to Lowe (1977), $\gamma$ in the psychometric constant (Pa °C$^{-1}$), $c_p$ is the heat capacity of

7    air (J kg$^{-1}$ K$^{-1}$), $\rho$ is the density of air (kg m$^{-3}$), $V$ is the vapour pressure deficit (Pa) and $r_a$ is

8    the aerodynamic resistance (s m$^{-1}$). To calculate the $r_a$ for the snow surface, the roughness

9    length for heat and water vapour ($z_{0v}$, m) is calculated using (Voogt and Grimmond, 2000):

10    $$z_{ov} = z_{0m} \exp(-20),$$    (12)

11    where $z_{0m}$ is the roughness length for momentum (m).

12    *Change in snow water equivalent*

13    For the water mass balance calculations, the model adopts a 5-minute time step in order to

14    respond to precipitation and snowmelt events. When the surface is completely covered by

15    snow, the snow water equivalent of the $i$th surface type ($S_{WE,i}$) is calculated:

16    $$S_{WE,i}(t + \Delta t) = S_{WEi}(t) + (P_i + F_i - E_i - R_i - T_{R,i}).$$  (mm (5 min)$^{-1}$)    (13)

17    If melt occurs ($M_i > 0$) the water is held in the snowpack until the liquid water holding

18    capacity $C_i^R$ is exceeded. The excess water goes directly to runoff ($R_i$). If the surface is

19    partially covered with snow, the excess water is added to the snow-free surface storage ($S_i$)

20    and the snow-free surface equations are used (Järvi et al., 2011). If a negative $S_{WE,i}$ occurs, the

21    calculated evaporation is assumed to be too large and is reduced by an equivalent amount

22    (constrained by $E_i$).

23    Snow from paved and built surfaces ($T_{R,i}$) can be transported out from the study area. The

24    amount removed is calculated as amount of excess snow above a defined threshold ($S_{WE,Lim}$).

25    This behaviour is neighbourhood specific (e.g. city or neighbourhood ordinances, snow

26    clearance priorities). The $S_{WE}$ is assumed to be reduced to the $S_{WE,Lim}$ at the next site specific

27    snow clearing time period. People are also assumed to redistribute snow (e.g. paths are

28    cleared and the snow is piled elsewhere) within the study area, and this is considered via

29    depletion curves (eq. 15a-c).

1 The snowpack starts to form when the surface temperature $T_s < 0°C$ and under two

2 conditions: when solid precipitation occurs; and/or when water on a snow-free surface freezes

3 ($F_i$). The snow depth $s_d$ (mm) is:

4 $$s_{d,i} = S_{WE,i} \frac{\rho_w}{\rho_s}.$$ (14)

5 *Surface fraction of snow*

6 One of the most important factors controlling the energy balance and snowmelt is the

7 patchiness of snow (Swenson and Lawrence, 2012). This is particularly important in urban

8 areas, where snow clearing from streets and roofs takes place regularly (Semádeni-Davies,

9 1999). During the melt period, surface type specific depletion curves are used to approximate

10 the fraction of snow cover ($f_s$) as a function of $S_{WE}$ (e.g. Ek et al., 2003; Valeo and Ho, 2004).

11 These are a function of surface specific maximum snow water equivalent $S_{WE}^{max}$ that control

12 the initiation of snow patchiness (Swenson and Lawrence, 2012). For vegetated surfaces, the

13 Swenson and Lawrence's (2012) form of the function is used with coefficients estimated

14 using the data for vegetated surfaces from Ek et al. (2003):

15 $$f_{s,veg} = 1 - \left( \frac{1}{\pi} \text{acos} \left( 2 \frac{S_{WE,veg}}{S_{WE,veg}^{max}} - 1 \right) \right)^{1.7}$$ (15a)

16 As this function was developed for climate models its application to smaller scales does

17 require caution. For paved and built surfaces, the equations were derived from Valeo and

18 Ho's (2004) data:

19 $$f_{s,pav} = \left( \frac{S_{WE}}{S_{WE,pav}^{max}} \right)^2$$ (15b)

20 $$f_{s,bldg} = 0.5 \left( \frac{S_{WE}}{S_{WE,bldg}^{max}} \right) \qquad \frac{S_{WE}}{S_{WE,bldg}^{max}} < 0.9$$
$$f_{s,bldg} = \left( \frac{S_{WE}}{S_{WE,bldg}^{max}} \right)^8 \qquad \frac{S_{WE}}{S_{WE,bldg}^{max}} \geq 0.9$$ (15c)

21 The forms of the depletion curves are shown in Appendix B. The different curves between

22 vegetation and impervious surfaces are used as human activities redistribute snow. For

23 example, large roadside snow piles are created that melt slowly through the spring. In

24 contrast, during the accumulation period snow is assumed to fall evenly on all surfaces.

## 2.2 Measurement sites and measurements

The model is applied in two cities that typically have extended periods of snow cover: Helsinki and Montreal. As multiple observation sites with different land-cover characteristics are available in both cities, model development is conducted independently of evaluation.

### 2.1.1  Helsinki, Finland

Meteorological and hydrological observations from three areas of Helsinki are used (Fig. 1). At the Kumpula (Ku, SMEAR III) site both meteorological forcing and evaluation data are measured (Järvi et al., 2009a). In addition, the observed runoff from Pasila (Pa) and Pihlajamäki (Pi) catchments are used for model development and evaluation. Ku is located 4 km north-east of the Helsinki city centre in a suburban area and 3.8 km from Pa and Pi (Fig. 1). Both Pa and the built sector of Ku (Ku1) have large areas of impervious surfaces (62%). At both sites, the buildings are mostly office buildings with mean height of 15 m (Pa) and 11 m (Ku1). Pa has pedestrian areas at two heights with extensive concrete surfaces creating a complex morphology. The other two sectors around the SMEAR III flux tower (Ku2, Ku3) and the Pi catchment are more vegetated (Table 1). Pi, with 34% impervious surfaces, is a typical suburban area in Helsinki with multi-family block houses.

Tower based eddy covariance (EC) sensible and latent heat fluxes measured at 31 m, with an ultrasonic anemometer (Metek, USA-1) and a closed-path infrared gas analyser (LI-7000, respectively, Li-COR Biosciences, Lincoln, NE, USA) at Ku are used. Post-processing of the 10 Hz data use commonly accepted procedures described in detail in Järvi et al. (2009b) and Nordbo et al. (2012a).

Tower-top air temperature (platinum resistant thermometer, Pt-100, "*in-house*"), wind speed (Thies Clima 2.1x, Goettingen, Germany) and incoming and outgoing short- and long-wave radiation (CNR1, Kipp&Zonen, Delft, Netherlands) are used to force and test the model. Other forcing data measured on a nearby roof (24 m a.g.l.) include air pressure (Vaisala DPA500, Vaisala Oyj, Vantaa, Finland), relative humidity (Vaisala HMP243), and precipitation (rain gauge, Pluvio2, Ott Messtechnik GmbH, Germany). Snow depth measured next to the tower by the Finnish Meteorological Institute is used in the model evaluation.

Runoff was monitored at one minute intervals using a OCM Pro CF flow meter (Nivus GmbH, Eppingen, Germany) mounted in the two catchment storm flow discharge pipes from September 2010 to 30 April 2011 (See Table 2 for data availability). In Pi, excess pipe flow

was observed causing runoff at unexpected times. Because of the water quality observed, this is thought to be associated with pipe leakage in household water systems. From the beginning of September, the excess pipe flow observed was 0.0038 $m^3$ $s^{-1}$ which had increased to 0.0125 $m^3$ $s^{-1}$ by the end of the measurement campaign. This pipe flow was removed from the analysis when assessing the runoff as pipe leakage is not modelled currently.

### 2.1.2 Montreal, Canada

Two residential areas with impervious cover of 71 % (Rl, Rosemont-La-Petite-Patrie borough) and 49 % (Pr, Pierrefonds-Roxboro borough) 18 km apart were modelled (see Bergeron and Strachan (2012) for map). The more densely populated Rl has two to three storey buildings, whereas the suburban Pr is a single family house residential area (Table 1).

At both sites, a tower mounted (26 m a.g.l.) sonic anemometer (CSAT3, Campbell Scientific Canada Corp., Edmonton, AB, Canada) and an open-path infrared gas analyser (LI-7500, Li-COR Biosciences, Lincoln, NE, USA) provided the 20 Hz data that are post-processed to EC fluxes of sensible and latent heat (Bergeron and Strachan, 2012). Forcing data of air temperature and relative humidity (HMP45C-212 at Rl, HMP45C at Pr, Campbell Scientific Canada Corp.), pressure (Barometric pressure sensor, RM Young Model 61205V, RM Young Company, Michigan, USA) and radiation (CNR1) are from the EC tower at 25 m a.g.l. Snow depths were monitored in the backyard of Pr and on the roof at Rl with snow ranging sensors (SR5, Campbell Scientific Canada Corp.). Snow properties, including snow density and albedo, were regularly (weekly: 2007/08 winter or bi-monthly: 2008/009 winter) observed for undisturbed snow, sidewalks, lawns and rooftops. Observations from Coteau-du-Lac (35 km southwest from Pr) and Pierre Elliot Trudeau Airport data (7 km from Pr and 16 km from Rl) (National Climate Data and Information Archive of Canada, 2013) are used to create a precipitation dataset with separation of snow/rain.

### 2.3. Model runs

In Helsinki, SUEWS was run for Ku for three years (January 2010 till December 2012) and for the two catchments for 16 months (January 2010 – April 2011, as observations are available for a shorter period). At all three sites, the first seven months are a spin-up period for the model that is neither used in model development nor testing. The spin-up time allows the model to become independent of the initial conditions set by the user. Even in urban areas, soil moisture initial state has a large impact on urban land surface model performance

1 (Best and Grimmond, 2013). The remainder of the periods are used for model development

2 and evaluation. In Ku, data prior to 2012 are used to develop and adjust model parameters:

3 $Q*$, upward shortwave radiation, and upward and downward long wave radiation are used to

4 adjust the snow, and surface albedo (Eq. 3 and 4), and $Q_H$ and $Q_E$ to test the

5 parameterizations for $Q_M$ and $\Delta Q_{S,I}$ (Eq. 5 and 6). The runoff measured in the denser

6 catchment (Pa) is used to constrain the temperature and radiation melt rates (Eq. 6), retention

7 capacity of the snow (Eq. 8) and the limit for the liquid precipitation. $Q^*$ and its components,

8 $Q_H$ and $Q_E$, the snow depth from Ku in 2012, and the runoff from the medium-intensity

9 catchment are used to independently evaluate the model.

10 The meteorological data measured at the Ku site are used to force the model for all three

11 Helsinki sites. The data are gap filled using the procedures described in Järvi et al. (2012).

12 Due to the very different characteristics surrounding the Kumpula tower, the model is run for

13 the three surface cover areas within a 1 km radius circle. The flux time series evaluated

14 against observations are combined from the surface cover areas (Ku1-3) based on the

15 prevailing wind direction.

16 In Montreal, only the first month of the 22 months (December 2007 till September 2009) is

17 used as a spin-up. The short spin-up time is chosen to allow two snow melt periods in model

18 development and testing. The remainder of the suburban dataset ($Q*$, $Q_H$, $Q_E$, snow depth,

19 snow density and albedo) is used for the model development: snow density and albedo are

20 used to determine the shape of the snow aging curves (Eq. 3, 4 and 9), $Q*$ the surface and

21 snow albedo, and $Q_H$, $Q_E$ the other snow related parameterizations. The urban site

22 observations are used for independent evaluation of the model. The model domain is a 1 km

23 radius circle around the flux tower.

24 The results are analysed by considering snow-free, cold snow and melting snow periods. For

25 snow-free, the simulated snow depth is zero, whereas the cold snow and melting snow

26 periods are separated by the air temperature 0°C.

27 **2.4 Evaluation statistics**

28 Several statistics are used to evaluate the model performance (e.g. Daley, 1991). Linear

29 regression is used to describe the linear dependence between the independent variable, in this

30 case the model output $X_{Mod}$, and the dependent variable, the observations ($X_{Obs}$). The slope

1     (*S*) relative to 1, and intercept (*I*) relative to zero, provide information on the model

2     performance. Further, goodness of fit is evaluated using the root mean square error (RMSE):

3     $$RMSE = \sqrt{\frac{\sum(X_{Mod}(t) - X_{Obs}(t))^2}{N}}$$     (16)

4     where *N* is the number of data points. Like the intercept in the linear regression, the RMSE

5     has the units of the variables being evaluated and it depends on the magnitude of the mean

6     variables. Therefore it is useful to normalize the RMSE (nRMSE) relative to the range of

7     values observed (Järvi et al. 2011):

8     $$nRMSE = \frac{RMSE}{X_{Obs,max} - X_{Obs,min}}$$     (17)

9     When comparing the performance of the model to simulate different variables, the RMSE can

10     also be normalized with the standard deviation of the observations $\sigma_{Obs}$ (Taylor 2001):

11     $$sRMSE = \frac{RMSE}{\sigma_{Obs}}$$     (18)

12     In addition, the mean bias error (MBE) between the modelled and observed time series is

13     considered:

14     $$MBE = \sum(\bar{X}_{Mod} - \bar{X}_{Obs}),$$     (19)

15     where the over bar indicates an average. Ideally, the RMSE, nRMSE, sRMSE and MBE

16     would all be zero.

17     **2.5 General weather conditions**

18     The weather conditions during the modelled period for Helsinki and Montreal are shown in

19     Figs. 2 and 3, respectively. Daytime solar radiation exhibits a strong seasonal pattern, with

20     the 15° latitudinal difference causing more rapid changes and stronger amplitude in Helsinki

21     than Montreal. In summer, $K{\downarrow}$ reaches 970 W m$^{-2}$ in Montreal, whereas in Helsinki the

22     maxima remain below 830 W m$^{-2}$. In winter, the solar radiation in Helsinki is very low (< 120

23     W m$^{-2}$), whereas Montreal peaks are below 400 W m$^{-2}$. Despite the difference in $K{\downarrow}$, air

24     temperatures are fairly similar in both cities. Daily maxima mean temperatures are around

25     26°C in summer, while the minimum daily mean temperature in winter in Helsinki is -20°C

26     and in Montreal -23°C. In both cities precipitation is quite evenly distributed throughout the

27     year.

1   During the three years of measurements, the daily snow depths in Helsinki are all below 0.8

2   m, with a longer snow period in winter 2010/2011 than 2011/2012. The timing of snowpack

3   formation depends strongly on the year. In 2010, it was initiated in November, whereas in the

4   following winter this was delayed until January 2012. This will have a large influence not

5   only on both natural energy and water exchanges, but also urban activities. In Montreal,

6   snowpack depth and timing has large variability between years; for example a 1 m snow pack

7   is observed in March 2008 with melting in late April, compared to only 0.6 m the next year,

8   with snow melted by the end of March.

9

10  **3. Results**

11  **3.1 Model optimization**

12  *Snow properties*

13  The time constants to describe the aging of snow, the minimum and maximum snow albedo,

14  and density were determined by optimization using observations undertaken at the suburban

15  site in Montreal (Pr). The observed snow properties are treated as averages from the

16  measured surface types, in order for them to be compatible with the scale of the simulations.

17  To evaluate the snow albedo, the observed reflected shortwave radiation ($K\uparrow$) in Helsinki in

18  2011 is also used. To assess the radiative exchanges, SUEWS is run using the radiation

19  measurements source area (99% FOV) estimated as a 31 m radius circle around the 31 m tall

20  measurement tower (Nordbo et al., 2012a). The surface cover characteristics are different for

21  this area to those within the turbulent flux source area; with 49% paved surface, 4%

22  buildings, 3% deciduous trees/shrubs and 44% grass.

23  Comparison of these observations with the Lemonsu et al. (2010) (hereafter Le10) aging

24  functions used for the suburban site in Montreal, shows that modifications to the coefficients

25  are needed for both snow albedo and density (Fig. 4). The Le10 maximum density of 350 kg

26  m$^{-3}$ is too small for the current observations. Thus, the maximum snow density is set to 400

27  kg m$^{-3}$; the minimum value $\rho_s^{min}$ is kept at 100 kg m$^{-3}$. In addition, the time constant $\tau_r$ is

28  decreased to 0.043. After these modifications, the simulated snow density follows the

29  behaviour of the median observations well (Fig. 4a). Similarly from the observations, the

30  minimum ($\alpha_s^{min}$) and maximum ($\alpha_s^{max}$) snow albedo are set to 0.18 and 0.85 respectively,

31  which differ from Le10 ($\alpha_n^{min}$= 0.15 - 0.30 across the different surface cover types). Le10's

14

1     snow albedo aging time constants ($\tau_f$ = 0.174, $\tau_a$ = 0.008) could not be fully evaluated due to

2     lack of data. However, $\tau_a$ compared to our observations is too small. When increased to 0.018,

3     $\tau_f$ decreases to 0.11. Again good correspondence between the observed snow albedo and

4     model output are seen (Fig. 4b), and between the observed and modelled $K\uparrow$ in Helsinki in

5     2012 (not shown). During the cold snow period, the linear fit statistics are $S$ = 0.68±0.02 W$^{-1}$

6     m$^2$, $I$ = 0.27±0.47 W m$^{-2}$ (RMSE = 11.3 W m$^{-2}$, $N$ = 2232), and during the warm snow period

7     $S$ = 0.50±0.01 W$^{-1}$ m$^2$ and $I$ = 0.85±0.47 W m$^{-2}$ (RMSE = 11.4 W m$^{-2}$, $N$ = 604). One likely

8     reason for the poorer model performance during the warm snow period is the sensitivity of

9     the albedo to the fraction of snow covered surface. In the model, the fraction of snow is

10    parameterized based on the maximum $S_{WE}$, but it is likely that this is site dependent at a

11    neighbourhood scale due to redistribution and transport of snow. However, as the other net

12    all-wave radiation components are larger in magnitude than $K\uparrow$, the negative bias during the

13    melting period is likely to have small impact on the available energy.

14    *Melt and freezing factors*

15    The freeze and melt factors ($a_r$ and $a_t$), representative for the neighbourhood scale, are

16    optimized using runoff from Pa and snow depth from Ku (Helsinki). SUEWS was run using

17    $a_r$ values between 0.0008 and 0.002 mm W$^{-1}$ h$^{-1}$ using 0.0001 mm W$^{-1}$ h$^{-1}$ resolution, and $a_t$

18    between 0.05 and 0.15 mm °C$^{-1}$ h$^{-1}$ with 0.01 mm °C$^{-1}$ h$^{-1}$ resolution. The 146 modelled

19    combinations were analysed with respect to the amount of accumulated melt water during the

20    snow covered period and the timing for complete snow melt (Table 3). The smallest

21    differences compared to the observations are obtained with $a_r$ = 0.0016 mm W$^{-1}$ h$^{-1}$ and $a_t$ =

22    0.12 mm °C$^{-1}$ h$^{-1}$. Thus, these are used in the model runs. Values are slightly larger, but of the

23    same order of magnitude, to those obtained for hourly factors at an Arctic watershed in

24    Alaska ($a_r$ = 0.001 mm W$^{-1}$ h$^{-1}$ and $a_t$ = 0.095 mm °C$^{-1}$ h$^{-1}$; Kane et al., 1997). Unfortunately,

25    no hourly values for urban areas were found in the literature. However, using these factors,

26    the daily melt rates are the same order of magnitude to those that have been typically reported

27    for urban areas (Bengtsson and Semádeni-Davies, 2011).

28    *Snow storage heat*

29    To determine the storage heat flux coefficients $a_1$, $a_2$ and $a_3$ for snow (Eq. 5) shallow water

30    values were used as an initial basis with $a_1$ = 0.50, $a_2$ = 0.21 and $a_3$ = -39.1 (Souch et al.,

31    1998). Given the assumption that the snow heat capacity is around half that of water (Rogers

32    and Yau, 1996), $a_1$ is set to 0.25 for snow. The other two coefficients ($a_2$ and $a_3$) are assessed

1    relative to their effect on the sensible heat flux by running SUEWS for Pr over a range of

2    values during the snow covered period. The homogenous area of Pr was used to optimize

3    $\Delta Q_{s,I}$. The RMSE between the observed and modelled $Q_H$ varies between 44.4 – 49.0 W m$^{-2}$

4    and MBE between -23.1 – 28.0 W m$^{-2}$, when $a_2$ varies between 0 and 1.2 and $a_3$ between -60

5    and 0 (Table 3). The optimal result with minimum RMSE = 48.2 W m$^{-2}$ and MBE = 0.19 W

6    m$^{-2}$ is obtained with $a_2$ = 0.60 and $a_3$ = -30. Thus, these coefficients are used in the model to

7    calculate the snow storage heat or the internal energy of the snow. The values imply a smaller

8    slope or fraction of radiative energy entering/leaving ($a_1$), a greater hysteresis ($a_2$) and a

9    similar phase or time lag ($a_3$) for snow relative to water. Heuristically this appears

10   appropriate.


11   **3.2 Model evaluation**

12   Table 4 lists the parameters, both for the snow covered and snow-free surface, used in the

13   model runs. The snow parameters are optimized (Section 3.1), whereas the limit values for

14   the snow transport ($S_{WE,Lim}$) were estimated based on maximum mass allowances of water at

15   the Pa catchment. The same values were used at all sites as no additional information was

16   available. Sensitivity analyses (Section 3.4) suggest the model is fairly insensitive to $S_{WE,Lim}$

17   despite the expectation for values to be neighbourhood specific.

18   **3.2.1. Surface runoff**

19   Figure 5 shows the daily observed and modelled runoff from the two catchments in Helsinki.

20   The grey line separates the non-snow and snow related runoff as the continuous winter snow

21   cover formed on 18 November 2010. At both sites, the model simulates the snow melt

22   induced runoff well, reproducing both the spring melt peak and the recession in April. When

23   the model is run treating the catchments as a whole, it tends to overestimate the runoff peaks

24   and to be flashier than observations (Fig. 5), which have smaller but longer runoff peaks.

25   Partly this can be explained by the absence of time lags for the water to move from the most

26   distant points (hydrologically and hydraulically) because the catchment is modelled as one

27   unit (in the current setup). However, in terms of hourly performance, the correlation between

28   the observed ($R_{obs}$) and modelled ($R_{mod}$) runoff is good with $S$ = 1.20 (mm h$^{-1}$)$^{-1}$ and $I$ = -0.01

29   mm h$^{-1}$ (RMSE = 0.14 mm h$^{-1}$, $r$ = 0.75) in Pa, and $S$ = 1.24 (mm h$^{-1}$)$^{-1}$ and $I$ = 0.02 mm h$^{-1}$

30   (RMSE = 0.16 mm h$^{-1}$, $r$ = 0.60) in Pi. The coefficients are calculated for periods when both

31   $R_{mod}$ and $R_{obs}$ are non-zero (675 and 760 hours in Pa and Pi, respectively). In Pa, the model

1    underestimates the cumulative runoff over the snow covered periods by 3 % as $R_{mod}$ = 82 mm

2    and $R_{obs}$ = 85 mm (Fig. 6). In Pi, the cumulative runoff is overestimated by 19% as $R_{mod}$ = 97

3    mm and $R_{obs}$ = 81 mm.

4

5    Before the continuous snow cover, the model performs similarly at both catchments. Notably,

6    the model overestimates runoff at Pi with high intensity precipitation. The overestimation is

7    seen in the linear correlation between $R_{obs}$ and $R_{mod}$ as $S$ = 1.29 (mm h$^{-1}$)$^{-1}$ and $I$ = 0.04 mm h$^{-}$

8    $^{1}$ (RMSE = 0.20 mm h$^{-1}$, $r$ = 0.68, $N$ = 668) as well as in the modelled cumulative runoff,

9    which is 47% higher than the observed in Pi (27 and 42 mm, respectively) (not shown). In Pa,

10    $S$ = 1.26 (mm h$^{-1}$)$^{-1}$ (RMSE = 0.20 mm h$^{-1}$, $r$ = 0.90, $N$ = 743), and the cumulative runoff is

11    4% underestimated by the model ($R_{obs}$ = 84 mm and $R_{mod}$ = 88 mm). Some of these

12    differences are caused by the forcing precipitation and other meteorological variables being

13    from the flux site Ku. This would particularly affect the model performance during

14    convective precipitation, which accounts for 88% of the precipitation events between April

15    and September (Punkka and Bister, 2005).

16    **3.2.2. Snow depth**

17    The model calculates snow water equivalent ($S_{WE}$) and snow depth ($s_d$) separately for each

18    surface type. Due to snow removal and the different surface characteristics, $s_d$ behaves

19    differently for the vegetated and built surfaces. This can be seen when the modelled $s_d$ for

20    each surface (paved, building, grass and tree) is plotted with the observations for Helsinki

21    (Fig. 7) and Montreal (Fig. 8). Unfortunately, the observations are each representative of

22    individual point and surface types, whereas the model values are for the different surface

23    types at the neighbourhood scale. Thus, some differences between the modelled and observed

24    $s_d$ are expected.

25    In Helsinki, the point observations are made in an open space that corresponds most

26    appropriately to the modelled grass surface. Data for 2011 and 2012 are plotted separately as

27    the first year is used in the model parameter determination whereas the latter is an

28    independent dataset (Fig. 7). In both years, the model reproduces the accumulation of snow

29    and melt events well, but underestimates the snow depth by 84 mm on average compared to

30    the observations. The measured maximum snow depth in 2011 is 720 mm, whereas the

31    modelled snow depth above grass is 587 mm. Similarly, for 2012 the observed depth is 630

32    mm and the modelled value is 504 mm. This underestimation is caused by either the

1    underestimation of modelled $S_{WE}$ or by overestimation of snow density as the snow depth is a

2    function of these two variables (Eq. 14). The model starts to accumulate snow four days later

3    than the observations in January 2012, but later in the year the observed and modelled snow

4    cover appear on the same date (29th November). In 2011, the snow melt is observed to have

5    ended on 15th April, five days earlier than simulated, whereas in 2012 the snow melt finished

6    on 12th April, one day later than modelled.

7    For Montreal, $s_d$ is calculated separately for the suburban (Pr) and urban (Rl) sites for January

8    2008 – April 2009. In Pr, the observations are made on lawn corresponding to the modelled

9    grass surface (Fig. 8a). The model follows the accumulation and melt events well, but like

10   Helsinki, snow depths are underestimated especially in the 2007 – 2008 winter. The

11   maximum observed $s_d$ is 1020 mm, while 670 mm was modelled for grass. In winter 2008 –

12   2009, the maximum observed and simulated snow depths are 665 and 460 mm. In 2008, the

13   modelled snow starts to accumulate on the same day (8th December) as observed. Snow melt

14   is completed on 20th April 2008, which is three days after the modelled date. In 2009 the

15   modelled snow melt finishes one day before observed (30th March).

16   In Rl, $s_d$ is observed on a building roof. This has both lower snow amounts and earlier melt

17   compared to the lawn observations in Montreal (Fig. 8b). The model simulates this behaviour

18   well, but again under predicts the depths. The observed $s_d$ maxima are 390 and 415 mm for

19   the two winters, while 301 and 285 mm are modelled, respectively. Accumulation of snow

20   takes place on the correct day in Rl, and the snow melts on the same day as observed (26

21   March) in 2008, and nine days later (7 March) in 2009 than observed.

22   The underestimation of $s_d$ is also impacted by the precipitation measurements, as the

23   difference between observed and modelled values begins during the snow accumulation

24   period. Precipitation measurements are known to underestimate snowfall especially due to

25   wind effects (Goodison et al., 1998; Savina et al., 2012).

26   **3.2.3. Turbulent and radiative energy fluxes**

27   The simulated $Q^*$, $Q_H$ and $Q_E$ are assessed for snow-free, cold snow and warm snow periods

28   (Table 5, Fig. 9), with the diurnal behaviour of both the observed and modelled fluxes for the

29   independent datasets in Helsinki and Montreal considered (Figs. 10 and 11).

30   Generally, the best simulated flux of the three is $Q^*$ independent of whether there is snow on

31   the ground or not. For the cold and warm snow periods, the RMSE varies between 27 – 41 W

1    m$^{-2}$ (nRMSE = 0.037 – 0.061) and 31 – 41 W m$^{-2}$ (nRMSE = 0.041 – 0.057) across the sites.

2    At all sites, $Q^*$ is underestimated in cold snow conditions with MBE between -34 and -13.5

3    W m$^{-2}$. Mostly this underestimation is related to the downward long-wave radiation that is

4    calculated from air temperature and relative humidity (Loridan et al., 2011 - who suggest that

5    use of cloud cover data as input with this technique is better). This parameterization works

6    less well in cold conditions than above 0 °C.  In Montreal, the warm snow underestimation is

7    even larger (MBE = -37 to -25 W m$^{-2}$), compared to Helsinki where the underestimation

8    decreases to -5 – -3 W m$^{-2}$. Especially during the warm snow periods, the fraction of snow

9    cover plays an important part in the model performance. It affects both the snow albedo and

10   outgoing long-wave radiation via surface temperature. The best performance for $Q^*$ is under

11   snow-free conditions, when the MBE is between -10 and 8 W m$^{-2}$ and the nRMSE is clearly

12   lower than for the periods with snow cover (Fig. 9a).

13   The scatter in the model performance is larger for $Q_E$ than for the other energy balance

14   components, with cold snow periods having the best and warm snow periods the poorest

15   model performance (Fig. 9c).  The RMSE during cold snow varies between 9 – 12 W m$^{-2}$

16   (nRMSE = 0.038 - 0.059), and for warm snow between 22 - 34 W m$^{-2}$ (nRMSE = 0.071 –

17   0.170). The increase in RMSE during warm snow periods is understandable as the energy

18   consumed in melting snow and freezing melt water is higher and thus errors in the degree-

19   day-method propagate more easily to $Q_E$ (as well as to $Q_H$). During melting periods there can

20   be advection from snow-free surfaces to the snowpack altering the energy balance as

21   specified in Eq. (1) (Bengtsson and Semádeni-Davies, 2011). MBE varies between -11 – 4 W

22   m$^{-2}$ when there is snow on ground. During snow-free periods, the model underestimates $Q_E$ at

23   all sites with MBEs between -27 – -11 W m$^{-2}$, RMSEs between 26 – 35 W m$^{-2}$, and nRMSE

24   between 0.058 – 0.066.

25   In SUEWS, $Q_H$ is calculated as a residual from other energy fluxes; therefore the net error

26   accumulates in $Q_H$. Despite this, the model is able to simulate its behaviour well. When there

27   is snow on ground, the RMSE varies between 23 – 50 W m$^{-2}$ and nRMSE between 0.067 and

28   0.118. During the cold snow periods, the simulated heat fluxes are slightly better than during

29   warm snow periods, similar to $Q_E$. The model overestimates $Q_H$ during snow cover, except in

30   Rl during cold snow periods, and MBEs vary between -25 – 9 W m$^{-2}$. In summer, the

31   performance of the model in simulating $Q_H$ improves following the performance of $Q^*$ and

32   $Q_E$.

1    The model performance for the energy fluxes is more dependent on the period of analysis

2    than the site where it is run. An exception to this is $Q_H$ at R1, where the model overestimates

3    and shifts the diurnal peak flux earlier compared to the observations (Fig. 11). This appears

4    whether there is snow on ground or not, suggesting that this is caused by the snow-free

5    storage heat flux which is underestimated or anthropogenic heat flux that is overestimated by

6    the model. RMSEs obtained for the warm snow periods in Pr are higher than Le10 obtained

7    for the same suburban area in Montreal using the Town Energy Balance model in spring

8    2005. However, direct comparisons are difficult as in their one month of observations snow

9    cover is present only on some days compared to the longer time period evaluated here.


10   **3.3 Energy balance of urban snow covered surface**

11   Snow cover and the related energy storage and the energy related to phase change alter the

12   surface energy balance. The components at the most built-up site Rl are evaluated here (Fig.

13   12). During cold snow periods, the daytime energy balance is dominated by the net all-wave

14   radiation ($Q^*$) and the sensible heat flux ($Q_H$), reaching 119 W m$^{-2}$ and 113 W m$^{-2}$. $Q_H$ is

15   fuelled by both $Q^*$ and $Q_F$ (reaching 46 W m$^{-2}$), and it accounts on average for 68% of the

16   daytime (10:00 – 15:00) available energy. The dominance of $Q^*$ and $Q_H$ are typical also for

17   natural cold snow packs (e.g. Oke, 1987). Only 12% of $Q^* + Q_F$, is dissipated by evaporation,

18   whereas the storage fractions are 10 and 8% at the snow and snow-free surfaces, respectively.

19   At night, on the other hand, the urban surface loses long-wave radiation causing the internal

20   energy of the snow to decrease i.e. the cold content of the snow increases. At the same time,

21   the snow-free surface loses some energy (around 10 W m$^{-2}$) and both $Q_F$ and $Q_E$ remain

22   positive (by more than 10 W m$^{-2}$), with $Q_H$ less than 5 W m$^{-2}$.

23   During warm snow periods, $Q^*$ is clearly the most important component of the surface energy

24   balance reaching 200 W m$^{-2}$ in daytime. Now the daytime $Q_F$ is slightly smaller than during

25   the cold periods reaching 35 W m$^{-2}$. Most of the energy, but clearly less than during the cold

26   snow period, is partitioned to $Q_H$ (46%), with the second largest contribution going to snow-

27   free surface heat storage (29%). Evaporation consumes 17% of the energy, and only 4% and

28   3% is stored in the snow and consumed by snow melt. The largest $Q_H$ and $\Delta Q_S$ are consistent

29   with the observations obtained by Le10 at the suburban site, although they documented a

30   larger contribution going to snow related processes than to evaporation. Moreover, the

31   modelled fractions during the snow covered periods are of the same order of magnitude as

32   obtained for observations at the same site (Bergeron and Strachan, 2012).

1   When the ground is free of snow, most energy ($Q^* + Q_F$) again goes to $Q_H$ (188 W m$^{-2}$, 45%)

2   followed by the storage heat flux (175 W m$^{-2}$, 42%). Due to the high impervious nature of the

3   surface, daytime $Q_E$ reaches 50 W m$^{-2}$, which is only 12% of the available energy. The

4   resulting daytime Bowen ration ($Q_H/Q_E$) is 3.7, which corresponds well with the expected

5   relationship of the Bowen ratio with the site's vegetation fraction (Loridan and Grimmond,

6   2012).


7 **3.4 Model sensitivity**

8   To better understand the impact of both the optimized values and those estimated (Table 4)

9   without detailed observation on the model performance, sensitivity analyses were undertaken.

10   The analysis included the power of the vegetation depletion curve (eq. 15a), limit for the

11   transport of snow from paved and roof surfaces ($S_{WE,Lim}$), snow heat storage ($a_2$, $a_3$) and the

12   melt water coefficients ($a_r$, $a_t$). SUEWS was run using the three independent datasets (Ku in

13   2012, Rl and Pi) changing the parameters by ±30% using a 10% step. The results were

14   compared to hourly measured $Q_H$, $Q_E$ and runoff and the RMSE determined for each site and

15   variable (Figure 13). The other parameters were held constant during each set of analyses.

16   The impact of the coefficients on heat storage in snow pack is shown only for $Q_H$ as their

17   effect on $Q_E$ and runoff is small or non-existent. $S_{WE,Lim}$ and the melt water coefficients have

18   the largest impact on the heat fluxes at both sites, whereas the smallest effect is for the power

19   used in the depletion curve. For runoff, the melt water coefficients have the largest effect.

20   The differences in model performances are relatively small in the context of the urban land-

21   surface model comparison (Grimmond et al. 2011) indicating that the model is fairly

22   insensitive to changes in the studied parameters.

23

24 **3   Conclusions**

25   The Surface Urban Energy and Water balance Scheme (SUEWS) is developed to simulate the

26   energy and water balances in cold climate cities with special attention on the simulation of

27   snow cover. The new model considers the accumulation of snow, snow properties including

28   snow water equivalent, snow depth, snow density and albedo, and snow melt and refreezing

29   of melt water based on an hourly degree-day method.  The development and independent

30   evaluation is undertaken using observations from three sites in Helsinki and two sites in

31   Montreal. Each of these sites varies in terms of surface cover characteristics. In Helsinki, the

observations include stormwater runoff from two catchments and turbulent fluxes of sensible and latent heat from one site. In Montreal, the observations include snow properties as well as the turbulent fluxes at both sites.

The model developments include an improved description of vegetation phenology (LAI) in cold climate cities. The leaf-off period based on daily air temperature was accelerated, using a combination of daily air temperatures and day length. Updated aging functions for snow density and albedo in urban areas were developed based on snow observations in Montreal an improved equation for the degree day method was used to calculate snow melt and freezing of the melted water, and new parameter values developed to calculate the snow storage heat flux using the objective hysteresis model (OHM).

The enhanced model can correctly simulate the winter and springtime melt-related runoff, but the runoff peaks tend to be sharper than the observations partly due to the absence of time lag to let the water flow to the observation point at the catchment discharge point. Despite this, the modelled cumulative runoff during the snow covered periods corresponds well with the observations. The formation and melting of the snowpack is simulated well both in Helsinki and Montreal, but the snow depth is underestimated either due to overestimation of the snow density or underestimation of snow water equivalent. Following the hydrological variables, the net radiation and turbulent sensible and latent heat fluxes also are modelled well. The model simulates their diurnal behaviour throughout the year, but the largest uncertainties occur during the snow melt period at all sites. This is related to the uncertainties in determining the snow covered surface fractions, as well as the propagating uncertainties from the calculation of melt and freezing related energies based on the degree-day method.

The model can correctly simulate the energy and water cycles in cold climate cities and it can potentially be used independently in urban planning purposes or nested to a meso- or global scale atmospheric model. However, some of the parameterizations are still city and site dependent; more observations from cold climate cities are needed to create more generalized formulations.

8

## 9   References

10  Anderson, E. A.: A point energy and mass balance model of a snow cover, NOAA Technical

11  Report NWS 19, 61-62, 1976.

12  Auer, A. H.: The rain versus snow threshold temperatures, Weatherwise 27, 67, 1974.

13  Baker, D. G., Ruschy, D. L., and Wall, D. B.: The albedo decay of prairie snows, J. Appl.

14  Meteor. 29, 179-187, 1990.

15  Bengtsson, L.: The importance of refreezing on the diurnal snowmelt cycle with application

16  to a Northern Swedish catchment, Nord. Hydrol. 13, 1-12, 1982.

17  Bengtsson, L.: Modeling snowmelt induced runoff with short time resolution. Proceedings of

18  3rd International Conference of Urban Storm Drainage, Gothenburg, Sweden, 305-314, 1984.

19  Bengtsson, L. and Westerström, G.: Urban snowmelt and runoff in northern Sweden,

20  Hydrological Sciences 37, 263-275, 1992.

21  Bengtsson, L. and Semádeni-Davies, A. F.: Urban snow in Encyclopedia of Snow, Ice and

22  Glaciers, Eds. Singh, V. P., Singh, P., and Haritashya, U. K., Springer Science, 1211-1217,

23  2011

24  Bergeron, O. and Strachan, I. B.: Wintertime radiation and energy budget along an

25  urbanization gradient in Montreal, Canada, Int. J. Clim. 32, 137-152, 2012.

26  Best, M. J. and Grimmond, C. S. B.: Analysis of the seasonal cycle within the first

27  international urban land-surface model comparison, Boundary-Layer Meteorol. 146, 421-446,

28  2013.

29  Cline, D. W.:  Snow surface energy exchanges and snowmelt at a continental, midlatitude

30  Alpine site, Water Resour. Res. 33, 689-701, 1997.

1    Daley, R.: Atmospheric Data Analysis, Cambridge University Press, Cambridge UK, 1991.

2    Debele, B., Srinivasan, R, and Gosain, A. K.: Comparison of process-based and temperature-
3    index snowmelt modeling in SWAT, Water Resour. Manag. 24, 1065-1088, 2010.

4    Easton, Z. M., Gérard-Marchant, P., Walter, M. T., Petrovic, A. M., and Steenhuis, T. S.:
5    Hydrologic assessment of an urban variable source watershed in the northeast United States,
6    Water Resour. Res. 43, W03413, doi: 10.1029/2006WR005076, 2007.

7    Ek, M. B., Mitchell, K. E., Lin, Y., Rogers, E., Grunmann, P., Koren, V., Gayno, G., and
8    Tarpley, J. D.: Implementation of Noah land surface model advances in the National Centers
9    for Environmental Prediction operational mesoscale Eta model, J. Geophys. Res. 108 (22),
10   8851, doi: 10.1029/2002JD003296, 2003.

11   Grimmond, C. S. B., Cleugh, H. A., and Oke, T. R.: An objective urban heat storage model
12   and its comparison with other schemes, Atmos. Env. 25B (3), 311-174, 1991.

13   Grimmond, C. S. B., Blackett, M., Best, M. J., Baik, J.-J., Belcher, S. E., Beringer, J.,
14   Bohnenstengel, S. I., Calmet, I., Chen, F., Coutts, A., Dandou, A., Fortuniak, K., Gouvea, M.
15   L., Hamdi, R., Hendry, M., Kanda, M., Kawai, T., Kawamoto, Y., Kondo, H., Krayenhoff, E.
16   S., Lee, S.-H., Loridan, T., Martilli, A., Masson, V., Miao, S., Oleson, K., Ooka, R., Pigeon,
17   R., Porson, A., Ryu, Y.-H., Salamanca, F., Steeneveld, G. J., Tombrou, M., Voogt, J. A.,
18   Young, D. T., and Zhang, N.: Initial results from Phase 2 of the international urban energy
19   balance model comparison, Int. J. Climatol., DOI: 10.1002/joc.2227, 2011.

20   Goodison, B. E., Louie, P. Y. T., and Yang, D.: The WMO solid precipitation measurement
21   intercomparison, World Meteorological Organization, Instruments and observing methods
22   67, 1998.

23   Jacobson, C. R.: Identification and quantification of the hydrological impacts of
24   imperviousness in urban catchments: A review, J. Environ. Manage. 92 (6), 1438-1448, 2011.

25   Jin, J., Gao, X., Sorooshian, S., Yang, Z.-L., Bales, R., Dickinson, R. E., Sun, S.-F., and Wu,
26   G.-X.: One-dimensional snow water and energy balance model for vegetated surfaces.
27   Hydrol. Process. 13, 2467-2482, 1999.

28   Järvi, L., Hannuniemi, H., Hussein, T., Junninen, H., Aalto, P. P., Hillamo, R., Mäkelä, T.,
29   Keronen, P., Siivola, E., Vesala, T., and Kulmala, M.: The urban measurement station
30   SMEAR III: Continuous monitoring of air pollution and surface-atmosphere interactions in
31   Helsinki, Finland, Boreal Env. Res. 14 (Suppl. A), 86-109, 2009a.

1    Järvi, L., Mammarella, I., Eugster, W., Ibrom, A., Siivola, E., Dellwik, E., Keronen, P.,

2    Burba, G., and Vesala, T.: Comparison of net $CO_2$ fluxes measured with open- and closed-

3    path infrared gas analyzers in urban complex environment, Boreal Env. Res. 14, 499-514,

4    2009b.

5    Järvi, L., Grimmond, C. S. B., and Christen, A.: The surface urban energy and water balance

6    scheme (SUEWS): Evaluation in Los Angeles and Vancouver, J. Hydrol. 411, 219-237, 2011.

7    Järvi, L., Nordbo, A., Junninen, H., Riikonen, A., Moilanen, J., Nikinmaa, E., and Vesala, T.:

8    Seasonal and annual variation of carbon dioxide surface fluxes in Helsinki, Finland, in 2006-

9    2010, Atmos. Chem. Phys. 12, 8475-8489, 2012.

10   Kane, D. L, Gieck, R. E., and Hinzman, L. D.: Snowmelt modeling at small Alaskan Arctic

11   watershed, J. Hydrol. Eng. 2, 204-210, 1997.

12   Keskitalo, J., Bergquist, G., Gardeström, P., and Jansson, S.: A cellular timetable of autumn

13   senescence, Plant Physiology 139, 1635-1648, 1995.

14   Koivusalo, H. and Kokkonen, T.: Snow processes in a forest clearing and in a coniferous

15   forest, J. Hydrol. 262, 145-164, 2002.

16   Kustas, W. P., Rango, A., and Uijlenhoet, R.: Simple energy budget algorithm for the

17   snowmelt runoff model, Water Resour. Res. 30 (5), 1515-1527, 1994.

18   Lemonsu, A., Bélair, S., Mailhot, J., Benjamin, M., Chagnon, F., Morneau, G., Harvey, B.,

19   Voogt, J., and Jean, M.: Overview and first results of the Montreal Urban Snow Experiment

20   2005, J. Appl. Meteorol. Clim. 47, 59-75, 2008.

21   Lemonsu, A., Bélair, S., Mailhot, J., and Leroyer, S.: Evaluation of the Town Energy Balance

22   model in cold and snowy conditions during the Montreal Urban Snow Experiment 2005, J.

23   Appl. Meteorol. Clim. 49, 346-362, 2010.

24   Leroyer, S., Mailhot, J., Bélair, S., Lemonsu, A., and Strachan, I. B.: Modeling the surface

25   energy budget during the thawing period of the 2006 Montreal Urban Snow Experiment, J.

26   Appl. Meteorol. Clim. 49, 68-84, 2010.

27   Loridan, T., Grimmond, C. S. B., Offerle, B. D., Young, D. T., Smith, T., Järvi, L., and

28   Lindberg, F.: Local-scale Urban Meteorological Parameterization Scheme (LUMPS):

29   Longwave radiation parameterization and seasonality related developments, J. Appl.

30   Meteorol. Clim., DOI: 10.1175/2010JAMC2474.1, 2011.

1 Loridan, T. and Grimmond, C. S. B.: Characterization of energy flux partitioning in urban

2 environments: Links with surface seasonal properties, J. Appl. Meteorol. Clim. 51, 219-241,

3 2012.

4 Lowe, P. R.: An approximation polynomial for the computation of saturation vapor pressure,

5 J. Appl. Meteorol. 16, 100-103, 1977.

6 Martine, G. and Marshall, A.: State of world population 2007: Unleashing the potential of

7 urban growth, U.N. Popul. Fund, New York, 2007.

8 Martinec, J.: Hour-to-hour snowmelt rates and lysimeter outflow during an entire ablation

9 period, Snow cover and Glacier Variations, Proceedings of the Baltimore Symposium,

10 Maryland, IAHS Publ. 183, 1989.

11 Mitchell, V. G., McMahon, T. A., and Mein, R. G.: Components of the total water balance of

12 an urban catchment, Environ. Manage. 32 (6), 735-746, 2003.

13 Mitchell, V. G., Cleugh, H. A., Grimmond, C. S. B., and Xu, J.: Linking urban water balance

14 and energy balance models to analyze urban design options, Hydrol. Process 22, 2891-2900,

15 2008.

16 Nordbo, A., Järvi, L., and Vesala, T.: Revised eddy covariance flux calculation

17 methodologies – effect on urban energy balance, Tellus B 48, 18184, 2012a.

18 Nordbo, A., Järvi, L., Haapanala, S., Moilanen, J., and Vesala, T.: Intra-City Variation in

19 Urban Morphology and Turbulence Structure in Helsinki, Finland, Boundary-Layer

20 Meteorol., doi 10.1007/s10546-012-9773-y, 2012b.

21 Offerle, B., Grimmond, C. S. B., and Oke, T. R.: Parameterization of net all-wave radiation

22 for urban areas. J. Appl. Meteor. 42, 1157-1173, 2003.

23 Oke, T.: Boundary Layer Climates, Routledge, London, UK, 1987.

24 Punkka, A. J. and Bister, M.: Occurrence of summertime convective precipitation and

25 mesoscale convective systems in Finland during 2000-01, Mon. Weather Rev. 133, 362-373,

26 2005.

27 Rogers, R. R. and Yau, M. K.: A short course in cloud physics. Elsevier Science, Oxford,

28 UK, 1996.

1  Savina, M., Schäppi, B., Molnar, P., Burlando, P. and Sevruk B.: Comparison of a tipping-
2  bucket and electronic weighting precipitation gage for snowfall, Atmos. Res. 103, 45-51,
3  2012.

4  Semádeni-Davies, A. F. and Bengtsson, L.: Snowmelt sensitivity to radiation in the urban
5  environment, Hydrol. Sci. J. 43, 67-89, 1998.

6  Semádeni-Davies, A. F.: Snow heterogeneity in Luleå, Sweden, Urban Water 1, 39-47, 1999.

7  Semádeni-Davies, A. F. and Bengtsson, L.: The water balance of sub-arctic town, Hydrol.
8  Process. 13, 1871-1885, 1999.

9  Semádeni-Davies, A., Lundberg, A., and Bengtsson, L.: Radiation balance of urban snow: a
10  water management perspective, Cold Reg. Sci. Technol. 33, 59-76, 2001.

11  Souch, C., Grimmond, C. S. B., and Wolfe, C. P.: Evaporation rates from wetlands with
12  different disturbance histories: Indiana dunes national lakeshore, Wetlands 18, 216-229,
13  1998.

14  Sun, S., Jin, J., and Xue, Y.: A simple snow-atmosphere-soil transfer model, J. Geophys. Res.
15  104 (D16), 19587-19597, 1999.

16  Swenson, S. C. and Lawrence, D. M.: A new fractional snow-covered area parameterization
17  for the Community Land Model and its effect on the surface energy balance, J. Geophys. Res.
18  117, D21107, 2012.

19  Taylor K.E.: Summarizing multiple aspects of model performance in a single diagram, J.
20  Geophys. Res. 106, 7183-7192, 2001.

21  Tobin, C., Schaefli, B., Nicótina, L., Simoni, S., Barrenetxea, G., Smith, R., Parlange, M.,
22  and Rinaldo, A.: Improving the degree-day method for sub-daily melt simulations with
23  physically-based diurnal variations, Adv. Water Resour. 55, 149-164, 2013.

24  Valeo, C. and Ho, C. L. I.: Modelling urban snowmelt runoff, J. Hydrol. 299, 237-251, 2004.

25  Valtanen, M., Sillanpää, N., and Setälä, H.: Effects of land use intensity on stormwater runoff
26  and its temporal occurence in cold climates, Hydrol. Process., doi: 10.1002/hyp.9819, 2013.

27  Vargo, J., Habeeb, D., and Stone, Jr., B.: The importance of land cover change across urban-
28  rural typologies for climate modelling, J. Environ. Manage. 114, 243-252, 2013

29  Verseghy, D. L.: CLASS – A Canadian land surface scheme for GCMS. 1, Soil Model, Int. J.
30  Clim. 11, 111-133, 1991.

1    Vesala, T., Järvi, L., Launiainen, S., Sogachev, A., Rannik, Ü., Mammarella, I., Siivola, E.,

2    Keronen, P., Rinne, J., Riikonen, A., and Nikinmaa, E.: Surface-atmosphere interactions over

3    complex urban terrain in Helsinki, Finland, Tellus 60B, 188-199, 2008.

4    Voogt, J. A. and Grimmond, C. S. B.: Modeling surface sensible heat flux using surface

5    radiative temperatures in a simple urban area, J. Appl. Meteorol. 39, 1679-1699, 2000.

6

7

8

9

10

Table 1. Site characteristics of the observational sites. Surface cover fractions for the EC sites are calculated for 1 km radius circles, whereas the fractions of the catchments are for the actual catchment areas. In Kumpula, the area is divided into three surface cover areas (Ku1, Ku2 and Ku3). For the abbreviations see Appendix C.

| | Helsinki | | | | | Montreal | |
| --- | --- | --- | --- | --- | --- | --- | --- |
| | Kumpula | | | Pasila | Pihlajamäki | Urban | Suburban |
| Lat | 60.203°N | | | 60.199°N | 60.238°N | 45.457°N | 45.501°N |
| Lon | 24.961°E | | | 24.940°E | 25.014°E | 73.592°W | 73.811°W |
| Obs. | $Q^*, Q_H, Q_E$ | | | $R$ | $R$ | $Q^*, Q_H, Q_E$, met. | $Q^*, Q_H, Q_E$, met. |
| $z$ (m) | 31 | | | - | - | 25 | 25 |
| Site name | Ku1 | Ku2 | Ku3 | Pa | Pi | Rl | Pr |
| $\lambda_{pav}$ | 0.42 | 0.39 | 0.30 | 0.42 | 0.22 | 0.44 | 0.37 |
| $\lambda_{bldg}$ | 0.20 | 0.15 | 0.11 | 0.20 | 0.12 | 0.27 | 0.12 |
| $\lambda_{veg}$ | 0.38 | 0.46 | 0.59 | 0.38 | 0.66 | 0.29 | 0.50 |
| $\lambda_{everg}$ | 0.01 | 0 | 0.01 | 0 | 0.10 | 0 | 0.05 |
| $\lambda_{dec}$ | 0.21 | 0.20 | 0.30 | 0.24 | 0.30 | 0.03 | 0.15 |
| $\lambda_{igrass}$ | 0.15 | 0.20 | 0.21 | 0.10 | 0.02 | 0.20 | 0.25 |
| $\lambda_{grass}$ | 0.01 | 0.06 | 0.10 | 0.02 | 0.1 | 0.06 | 0.05 |
| $\lambda_{unman}$ | 0 | 0 | 0 | 0.02 | 0.14 | 0 | 0 |
| $\lambda_{water}$ | 0 | 0.01 | 0.00 | 0 | 0 | 0 | 0.01 |
| $z_h$ (m) | 10.4 | 11.5 | 12.6 | 15.2 | 10.8 | 7.9 | 6.4 |
| $z_t$ (m) | 10 | 8.8 | 8.5 | 8 | 8 | 13.0 | 13.8 |
| $p$ (# ha$^{-1}$) | 31 | 37 | 44 | 42 | 55 | 84 | 24 |
| $A$ (ha) | 44.7 | 78.2 | 78.2 | 23.8 | 44.8 | 314.2 | 314.2 |
| Reference | Järvi et al. (2009a) | | | - | - | Bergeron and Strachan (2012) | |

1 Table 2. Time period and the spin-up time of the model simulations. Data availability refers to

2 the number of 60 min periods when observations are available for the non-spin-up period. EC

3 is the eddy covariance fluxes ($Q_H$ and $Q_E$), $R$ is the runoff and $s_d$ the snow depth. A sub-set of

4 these data are used in parameter optimization and another for evaluation.

| | | Measurement period | Spin-up period | Data availability during non-spin-up (%) |
|---|---|---|---|---|
| Ku | EC | 2010-2012 | Jan - Aug 2010 | 44 |
| | $s_d$ | | | 100 |
| Pa | $R$ | Sep 2010 – Apr 2011 | Jan -Aug 2010 | 93 |
| Pi | $R$ | | | 86 |
| Pr | EC | Dec 2007 – Sep 2009 | Dec 2007 | 53 |
| | $s_d$ | | | 80 |
| Rl | EC | | | 36 |
| | $s_d$ | | | 85 |

5

6

7

8

9

10

11

12

13

14

15

16

17

18

1	Table 3. Results of the model optimization made for the snow storage heat and melt water

2	calculations. Different evaluation criteria for the components were used.

| | Range of tested values | Final value | Evaluation criteria | Range of the evaluation criteria | Site |
|---|---|---|---|---|---|
| $a_r$ | 0.0008-0.002 | 0.0016 | Cumulative $R/D_{sm}$ | -14 - -3/-7.6-16.1 (mm) | Pa, Ku |
| $a_t$ | 0.05-0.15 | 0.12 | Cumulative $R/D_{sm}$ | -14 - -3/-7.6-16.1 (mm) | Pa, Ku |
| $a_2$ | 0-1.2 | 0.5 | RMSE/MBE of $Q_H$ | 44.4-49.0/-23.1-28.0 (W m$^{-2}$) | Pr |
| $a_3$ | -60-0 | -30 | RMSE/MBE of $Q_H$ | 44.4-49.0/-23.1-28.0 (W m$^{-2}$) | Pr |

3

4

5

6

7

8

9

10

Table 4. Parameters used in SUEWS for surfaces that are buildings (bldg), pavement (pav), evergreen vegetation (everg), deciduous vegetation (decid), grass and water. If the vegetation is irrigated, different values to describe the canopy are used. Sources of the values are as in Järvi et al. (2011) unless indicated otherwise below. Where different values are used for the different sites, this is indicated for Helsinki (Hel), and for the two sites in Montreal (Rl and Pr). Variable notation is given in Appendix C.

| a) | Site | Units | Bldg | Pav | Everg. | Decid. | Irr. veg | Grass | Water |
|---|---|---|---|---|---|---|---|---|---|
| $S_i$ | | mm | 0.25 | 0.48 | 1.3 | 0.3-0.8 | | 1.9 | 0 |
| $S_{soil,i}$ | Hel/Rl | mm | 50 | 100 | 150 | 150 | 150 | 150 | - |
| | Pr | mm | 150 | 150 | 150 | 150 | 150 | 150 | - |
| $D_{0,i}$ | | mm | 10 | 10 | 0.013 | 0.013 | 10 | 0.013 | - |
| $b$ | | - | 3 | 3 | 1.71 | 1.71 | 0.013 | 1.71 | - |
| $C_i$ | | mm | 0 | 0 | 0 | 0 | 0 | 0 | 0 |
| $C_{soil,i}$ | Hel/Rl | mm | 50 | 100 | 150 | 150 | 150 | 150 | - |
| | Pr | mm | 150 | 150 | 150 | 150 | 150 | 150 | - |
| $\alpha_i$ | | - | 0.15 | 0.09[i] | 0.10 | 0.16[ii] | 0.19 | 0.19[ii] | 0.08[ii] |
| $\varepsilon_i$ | | - | 0.95 | 0.91 | 0.98 | 0.98 | 0.93 | 0.93 | 0.95 |
| $g_{i,max}$ | | mm s$^{-1}$ | - | - | 7.4 | 11.7 | 40 | 33.1 | - |
| ***Snow*** | | | | | | | | | |
| $S_{WE,0}$ | Hel | mm | 40 | 40 | 40 | 40 | 40 | 40 | 40 |
| | Mon | mm | 0 | 0 | 0 | 0 | 0 | 0 | 0 |
| $f_{s,i,0}$ | Hel | mm | 1 | 1 | 1 | 1 | 1 | 1 | 1 |
| | Mon | mm | 0 | 0 | 0 | 0 | 0 | 0 | 0 |
| $\rho_{s,0}$ | | kg m$^{-3}$ | 120 | 120 | 120 | 120 | 120 | 120 | 120 |
| $S_{WE,i}^{max}$ | | mm | 190 | 190 | 190 | 190 | 190 | 190 | - |
| $S_{WE,Lim}$ | | mm | 40 | 100 | | | | | |

**b) Overall area parameter values**

| | | | | | | | |
|---|---|---|---|---|---|---|---|
| $\alpha_s^{min}$ | 0.18 | $a_{0,\{wd,we\}}$ | 0.1 W m$^{-2}$ (p$^{-1}$ ha$^{-1}$)$^{-1}$[i] | $G_4$ | 3.36 g kg$^{-1}$ | $res_{cap}$ | 10 mm |
| $\boldsymbol{\alpha_s^{max}}$ | 0.85 | $a_{1,\{wd,we\}}$ | 9.9·10$^3$ Wm$^{-2}$ K$^{-1}$ (p$^{-1}$ ha$^{-1}$)$^{-1}$ | $G_5$ | 11.07°C | $res_{drain}$ | 0.25 mm h$^{-1}$ |
| $\varepsilon_s$ | 0.99 | $a_{2,\{wd,we\}}$ | 0.0102 Wm$^{-2}$ K$^{-1}$ (p$^{-1}$ ha$^{-1}$)$^{-1}$ | $G_6$ | 0.018 mm | $R_C$ | 1.0 mm |
| $\rho_e$ | 200 kg m$^{-3}$ | $b_{0,a}$ | -84.54 mm | GDD | 300 | $S_1$ | 0.45 mm |
| $\boldsymbol{\rho_s^{min}}$ | 100 kg m$^{-3}$ | $b_{1,a}$ | 9.96 mm K$^{-1}$ | $I_w$ | 0 mm | $S_2$ | 15 mm |
| $\boldsymbol{\rho_s^{max}}$ | 400 kg m$^{-3}$ | $b_{2,a}$ | 3.67 mm d$^{-1}$ | $K\downarrow_m$ | 1200 W m$^{-2}$ | $S_{Pipe}$ | 100 mm |
| $\tau_a$ | 0.018 | $b_{0,m}$ | -25.36 mm | $K_s$ | 0.0005 mm s$^{-1}$ | SDD | -450 |
| $\tau_f$ | 0.11 | $b_{1,m}$ | 3.00 mm K$^{-1}$ | LAI$_{max,everg}$ | 5.1 m$^2$ m$^{-2}$ | $T_{BaseGDD}$ | 5°C |
| $a_1$ | 0.25 | $b_{2,m}$ | 1.10 mm d$^{-1}$ | LAI$_{max,dec}$ | 5.5 m$^2$ m$^{-2}$ | $T_{BaseSDD}$ | 10°C |
| $a_2$ | 0.6 | $C_{min}^R$ | 0.05 mm | LAI$_{max,grass}$ | 5.9 m$^2$ m$^{-2}$ | $T_{BaseQF}$ | 18.2°C |
| $a_3$ | -30 | $C_{max}^R$ | 0.2 mm | LAI$_{min,everg}$ | 4.0 m$^2$ m$^{-2}$ | $T_{lim}$ | 2.2°C [iii] |
| $a_f$ | 1 | $G_1$ | 16.48 mm s$^{-1}$ | LAI$_{min,dec}$ | 1.0 m$^2$ m$^{-2}$ | $T_H$ | 40°C |
| $a_r$ | 0.0016 mm W$^{-1}$ h$^{-1}$ | $G_2$ | 566.1 W m$^{-2}$ | LAI$_{min,grass}$ | 1.6 m$^2$ m$^{-2}$ | $T_L$ | 10°C |
| $a_t$ | 0.011 mm °C$^{-1}$ h$^{-1}$ | $G_3$ | 0.216 kg g$^{-1}$ | $r_{s,max}$ | 9999 s m$^{-1}$ | $T_{step}$ | 300 s |

[i]Optimized using data from Helsinki; [ii]Vargo et al. (2013); [iii]Auer (1974)

1    Table 5. Model evaluation statistics based on performance relative to observations of net all

2    wave radiation ($Q^*$, W m$^{-2}$), sensible ($Q_H$, W m$^{-2}$) and latent heat fluxes ($Q_E$, W m$^{-2}$)

3    undertaken for two years in Helsinki (Ku11 for 2011 and Ku12 for 2012) and two sites in

4    Montreal (Pr and Rl). The statistics: RMSE is the root mean square error (W m$^{-2}$), nRMSE

5    the normalized RMSE (eq. 17), sRMSE (eq. 18) is RMSE normalized with standard deviation

6    of the observed value and $N$ is the number of points in the linear fit.

| | | Cold snow | | | | | Melting snow | | | | | Snow-free | | | | |
|---|---|---|---|---|---|---|---|---|---|---|---|---|---|---|---|---|
| | | RMSE | nRMSE | sRMSE | $N$ | MBE | RMSE | nRMSE | sRMSE | $N$ | MBE | RMSE | nRMSE | sRMSE | $N$ | MBE |
| Ku11 | $Q^*$ | 34.3 | 0.0445 | -1.3 | 1697 | -13.7 | 38.1 | 0.0492 | 0.9 | 1020 | -5.1 | 30.3 | 0.0303 | 0.43 | 5992 | 7.7 |
| | $Q_H$ | 29 | 0.0719 | 1.3 | 756 | -8.7 | 50.4 | 0.1009 | 0.95 | 435 | -16.7 | 37.5 | 0.0628 | 0.76 | 3069 | -1.1 |
| | $Q_E$ | 12.3 | 0.0378 | 0.72 | 613 | -2.1 | 23.7 | 0.0713 | 0.65 | 377 | -10.8 | 25.8 | 0.0584 | 0.64 | 2627 | -23.8 |
| Ku12 | $Q^*$ | 26.5 | 0.0371 | -0.7 | 2238 | -31 | 40.6 | 0.057 | 1.31 | 644 | -3.1 | 29 | 0.0302 | 0.37 | 5584 | 7.3 |
| | $Q_H$ | 23 | 0.0734 | 1.9 | 1056 | -24.6 | 37.9 | 0.0822 | 0.74 | 284 | -12.6 | 38.4 | 0.0555 | 0.74 | 3429 | -8.2 |
| | $Q_E$ | 9.7 | 0.0429 | 0.7 | 775 | -5.5 | 21.9 | 0.0974 | 0.58 | 221 | -10.5 | 26.5 | 0.0664 | 0.58 | 2868 | -27 |
| Pr | $Q^*$ | 38.3 | 0.055 | -6.34 | 2980 | -34.3 | 31.2 | 0.0411 | 0.42 | 1145 | -37.1 | 24.6 | 0.0276 | 0.21 | 6952 | -4.4 |
| | $Q_H$ | 32.5 | 0.0826 | 1.41 | 2177 | -8.4 | 45.7 | 0.1081 | 0.97 | 672 | -16.8 | 32.2 | 0.0698 | 0.67 | 5598 | -13.2 |
| | $Q_E$ | 11.8 | 0.0398 | 0.74 | 2063 | 1.7 | 34.1 | 0.1704 | 0.82 | 649 | 3.6 | 34.8 | 0.0662 | 0.59 | 5463 | -11.9 |
| Rl | $Q^*$ | 40.9 | 0.0613 | -57.64 | 2740 | -13.5 | 31.6 | 0.0422 | 0.5 | 965 | -25.4 | 26.7 | 0.0322 | 0.21 | 4521 | -9.4 |
| | $Q_H$ | 30.9 | 0.0673 | 0.64 | 1366 | 9.1 | 42.7 | 0.088 | 0.68 | 522 | -16 | 47.7 | 0.0857 | 0.53 | 3762 | -10 |
| | $Q_E$ | 8.6 | 0.0587 | 0.55 | 1292 | 1.2 | 23.3 | 0.1189 | 0.76 | 499 | 3.4 | 28.5 | 0.0654 | 1.05 | 3661 | -10.8 |

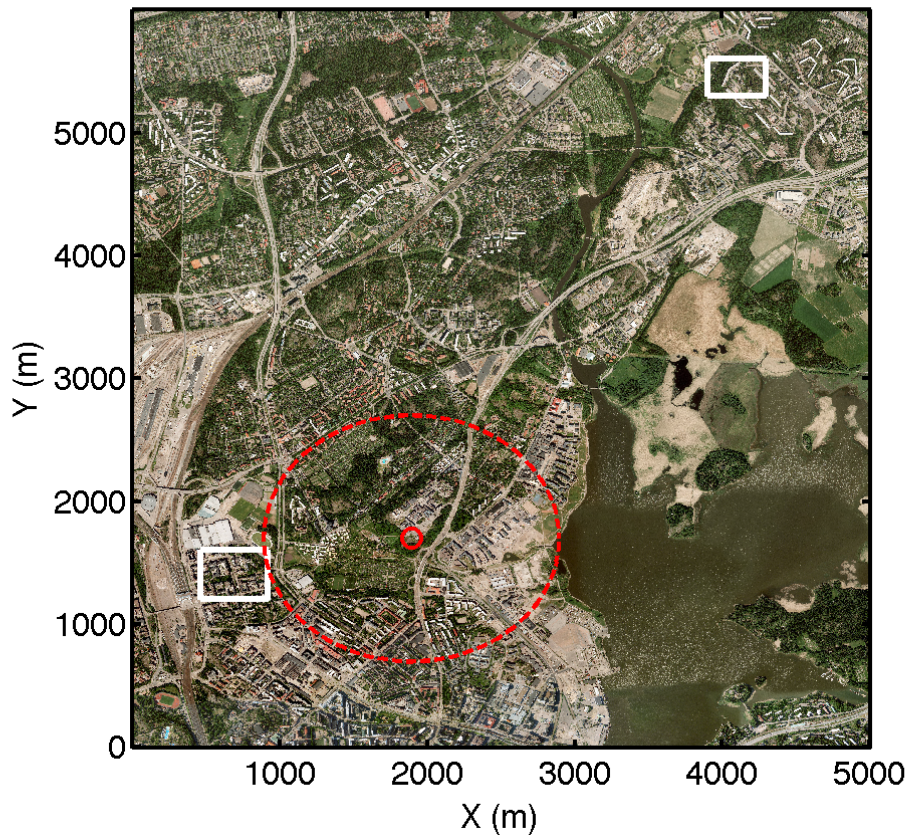7

8

9

10

11

12

13

14

15

1

Figure 1. Aerial photograph of the measurement locations in Helsinki. Red dot is the

SMEARIII-Kumpula site (Ku). The red dashed line is the 1 km radius circle that the surface

cover fractions are calculated for, and the white squares show the approximate locations of

the catchment areas (Pa left side and Pi top-right). © Kaupunkimittausosasto, Helsinki, 2011.
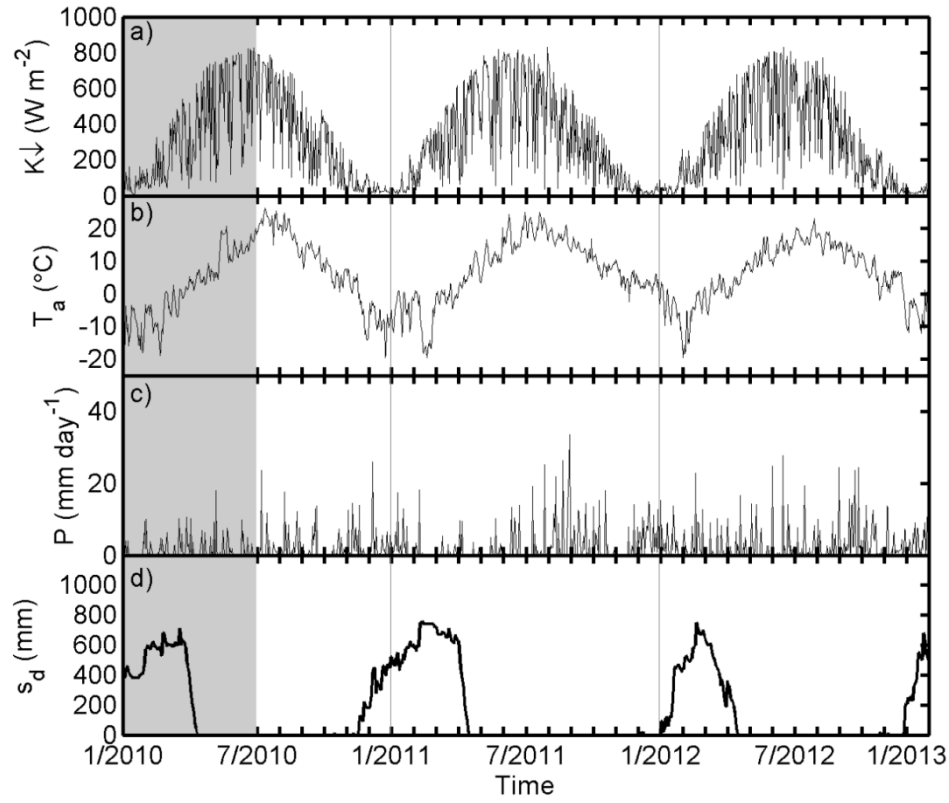
6

7

8

9

10

11

12

13

14

Figure 2. Time series of daily a) daytime (10:00 – 14:00) solar radiation ($K\downarrow$), b) air temperature ($T_a$), c) precipitation ($P$) measured in SMEAR III – Kumpula, and d) snow depth measured at Kumpula. Grey area shows the spin-up period.
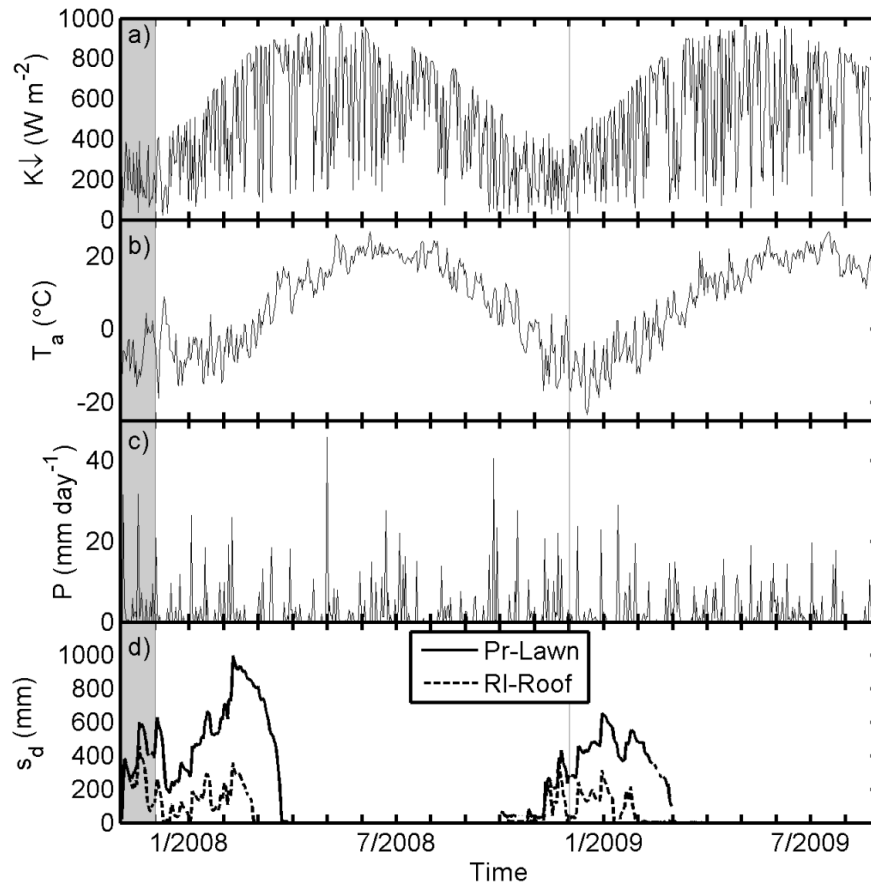
1

2　Figure 3. As Fig.2 but for Montreal measured at the suburban site (Pr) with snow depth

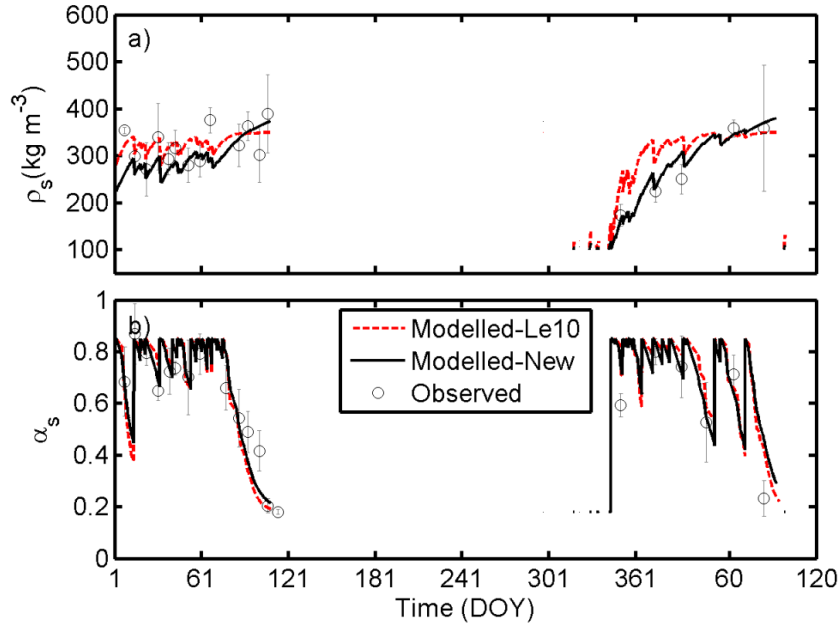3　measured in a suburban back lawn (Pr) and on an urban roof (Rl).

4

5

6

7

8

9

10

11

Figure 4. Observed and modelled a) snow density ($\rho_s$) and snow albedo ($\alpha_s$) at the suburban site in Montreal (January 2008 – April 2009). Observed values are the medians from four locations and the error bars show the quartile deviations. Aging functions proposed in Lemonsu et al. (2010) 'Le10' and in the current study ('New').

1

2

3
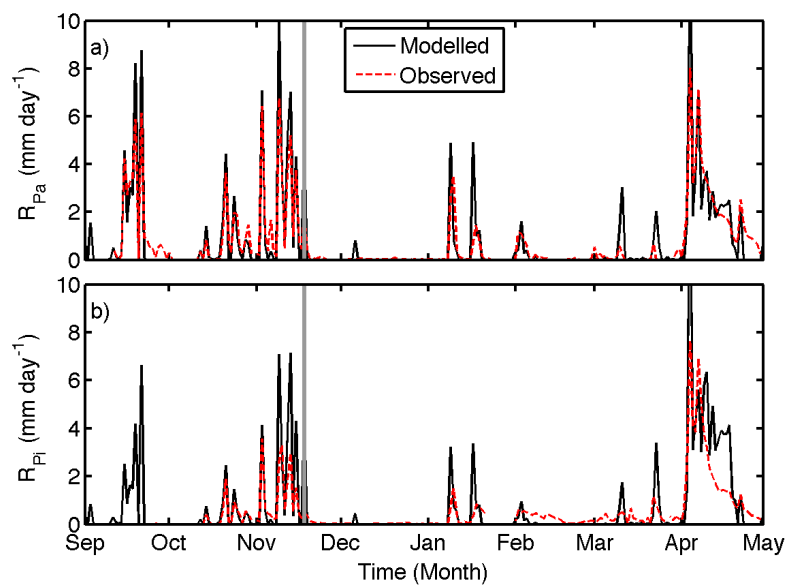
4

5

6

7

8

9

10

11

12

13

14

15

16

17

18

Figure 5. Modelled and observed runoff at a) Pa and b) Pi (independent) sites. Grey line indicates when the snow starts to accumulate on ground; the snow melts by the end of April.
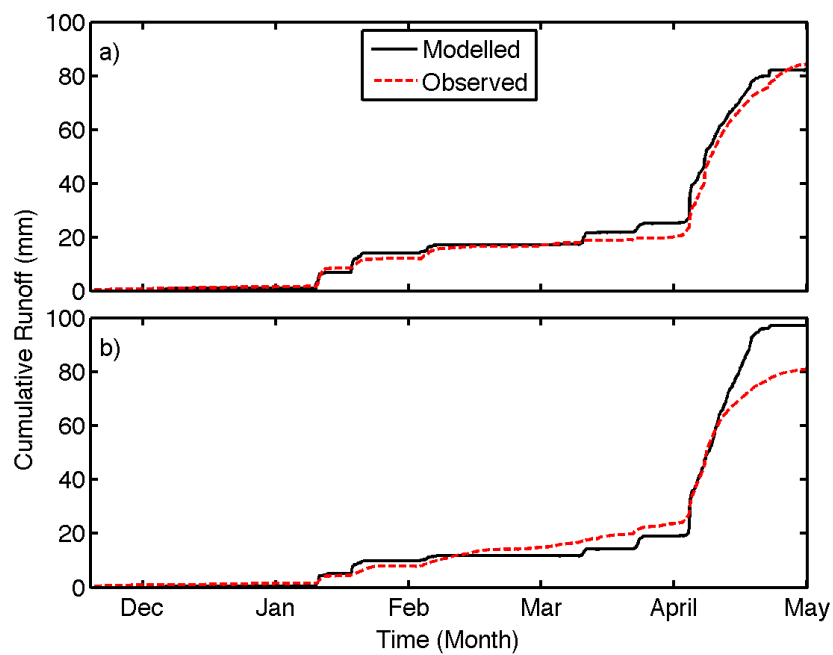
Figure 6. Modelled and observed cumulative runoff during the snow covered period (19 November 2010 – 31 April 2011) a) Pa and b) Pi (independent) catchments.

1

2

3

4
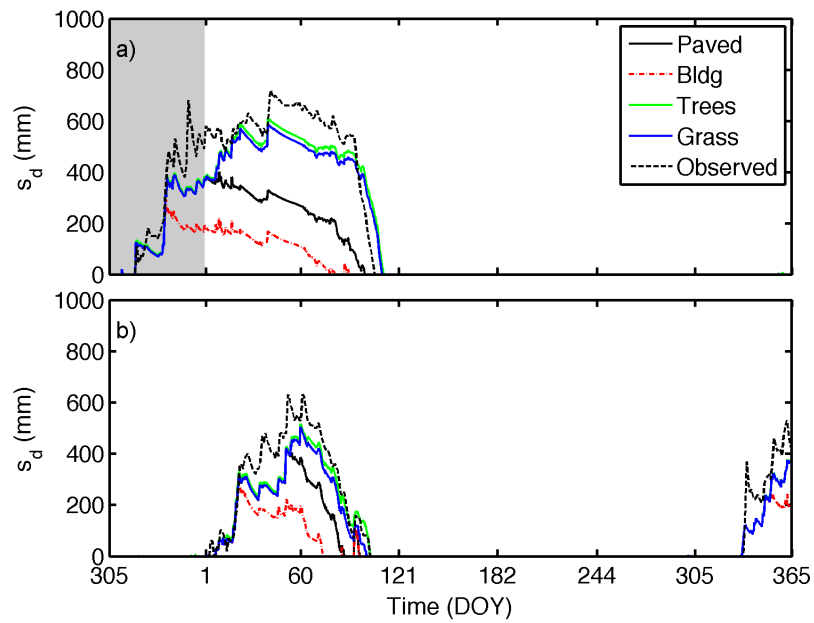
5

6

7

8

9

10

11

12

13

14

15

16

17

1



Figure 7. Simulated (by surface type) and observed snow depth in Helsinki in a) 2011 and b)
2012. Grey area shows the spin-up period.

2

3

4

5

6

7

8

9

10
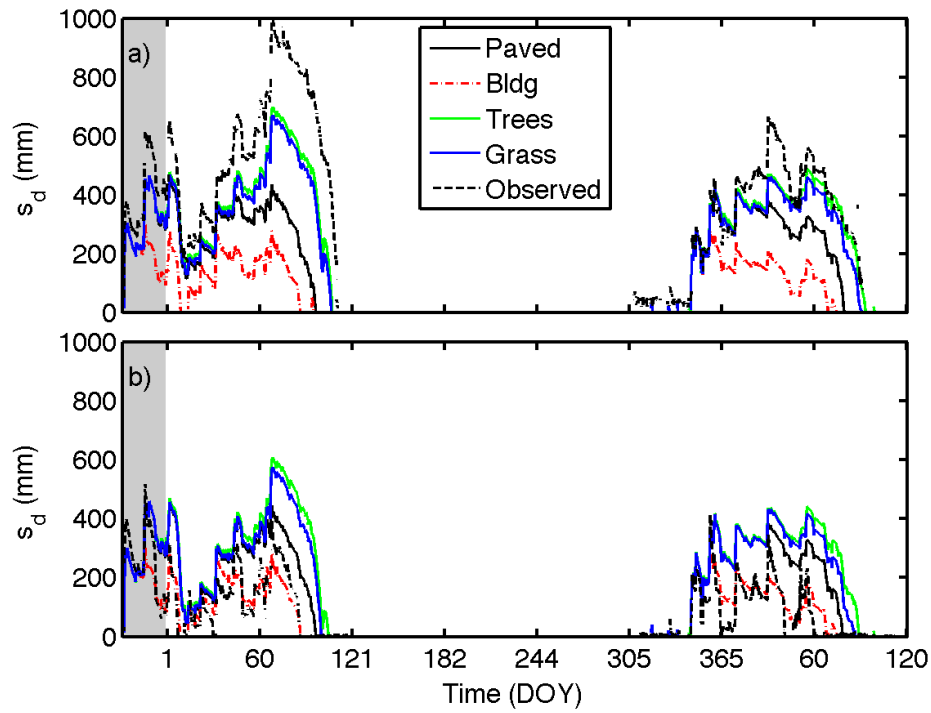
11

12

13

14

15

16

17

18

1



2

Figure 8. As Fig 7 for Montreal in 2008 – 2009 a) suburban site with observations above

(grass) lawn and b) urban site with (building) roof observations. Grey area shows the spin-up

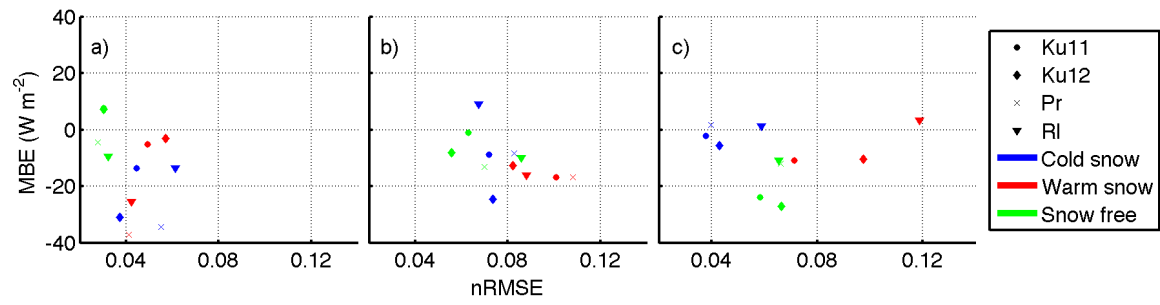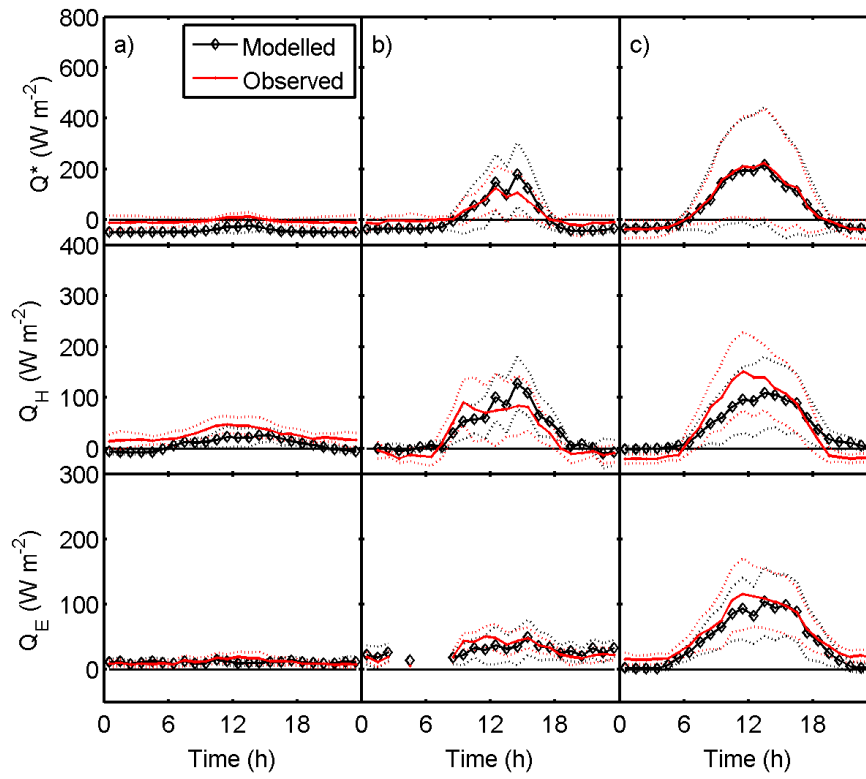period.

6

7

8

9

10

11

12

13

14

15

16

17

1



2

Figure 9. Model performance for the three periods a) cold snow, b) warm snow and c) snow-free. Mean bias error (MBE) versus normalized root mean square error (nRMSE) for different sites and for Ku separately (years 2011 (Ku11) and 2012 (Ku12)).

6

7

8

9

10

11

12

13

14

15

16

17

18

19

20

21

22

1



Figure 10. Diurnal behaviour of the measured and modelled net all-wave radiation ($Q^*$) and turbulent energy fluxes ($Q_H$ and $Q_E$) during a) cold snow, b) melting snow and c) snow-free periods in Helsinki in 2012. Only hours when observations are available were accounted. Dotted lines show the quartile deviations.

7

8

9

10

11

12

13
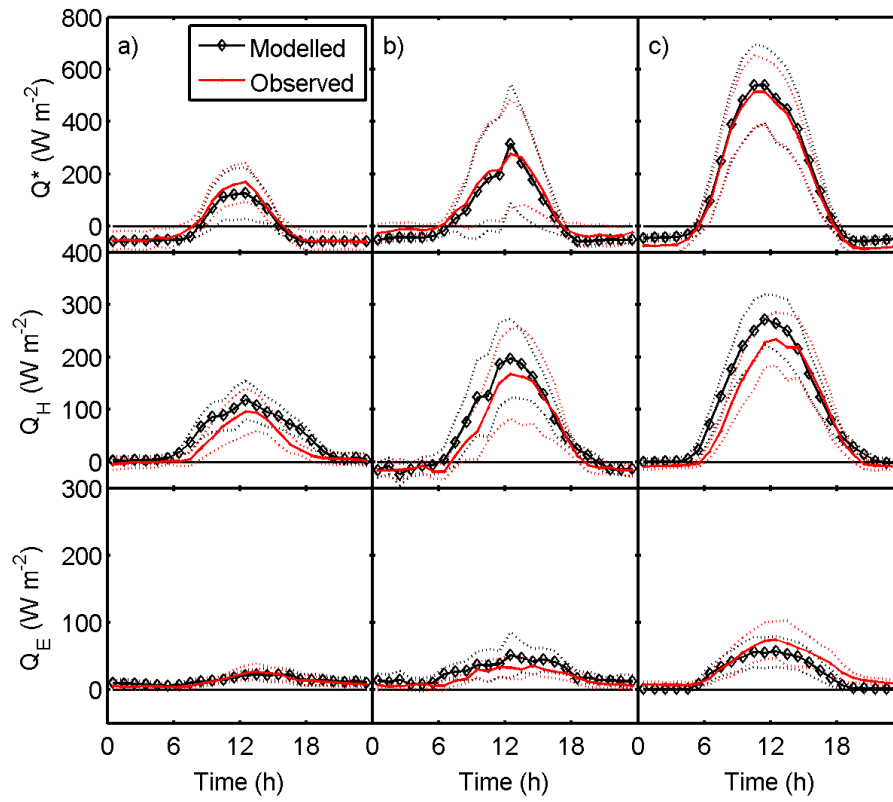
Figure 11. As Fig 10, for the urban site in Montreal (Rl) in 2008 - 2009.

1

2

3

4

5

6

7

8

9

10

11

12

13

14

15
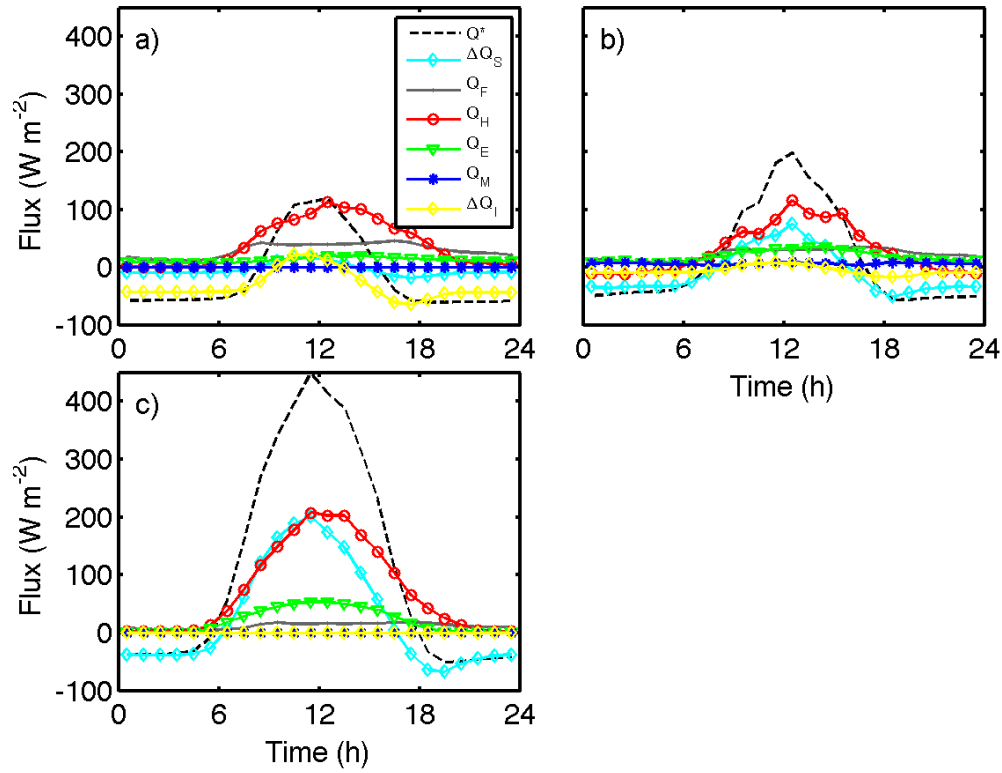
Figure 12. Energy balance at the urban site (Rl) in Montreal during a) cold snow, b) warm snow and c) snow-free periods. $Q^* =$ net all wave radiation, $\Delta Q_S =$ heat storage to snow-free surfaces, $Q_F =$ anthropogenic heat flux, $Q_H =$ sensible heat flux, $Q_E =$ latent heat flux, $Q_M =$ snow melt/freezing water related energy flux, and $\Delta Q_I =$ heat storage in snow pack.
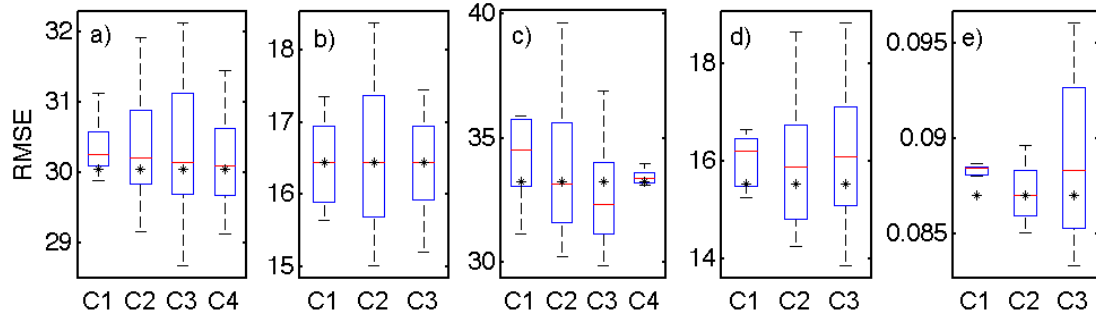
1
2  Figure 13. Boxplot of RMSE's of the sensitivity analysis made for a) $Q_H$ in Ku (W m$^{-2}$), b)

3  $Q_E$ in Ku (W m$^{-2}$), c) $Q_H$ in Rl (W m$^{-2}$), d) $Q_E$ in Rl (W m$^{-2}$) and e) runoff in Pi (mm h$^{-2}$). The

4  sensitivity are to changes in: the power in the depletion curve (eq. 15a) (C1), $S_{WE,Lim}$ (C2),

5  melt water coefficients ($a_r, a_t$) (C3), and storage heat flux coefficients ($a_2, a_3$) (C4). The final

6  model values are indicated (*). For other details see text.

7

8

9

10

11

12

13

14

15

16

17

18

19

20

21

22

23

1    Appendix A. Leaf area index (LAI)

2    In SUEWS, changes in phenology, such as growing season length, are allowed to vary from

3    year to year as a function of thermal conditions through growing degree days and senescence

4    degree days. The thermal thresholds are changed to be appropriate for a location (e.g.

5    latitude, continental vs. maritime climate) (Järvi et al., 2011). At high latitudes, air

6    temperature is a good proxy for leaf growth in spring, whereas the leaf-off is initiated by day

7    length (Keskitalo et al., 2005). However, air temperature still influences the rate of leaf fall.

8    Thus the functions to calculate daily leaf area index ($LAI_{d,i}$) are modified to take also the day

9    length into account according to

10
$$\begin{cases} LAI_{d,i} = LAI_{d-1,i}^{b1} GDD \cdot c_1 + LAI_{d-1}, \text{ leaf} - \text{on, } T_d > T_{BaseGDD} \\ LAI_{d,i} = LAI_{d-1,i}^{b2} SDD \cdot c_2 + LAI_{d-1}, \text{ leaf} - \text{off}, T_d < T_{BaseSDD}, \text{or} \\ LAI_{d,i} = LAI_{d-1,i} b_3 (1 - GDD) \cdot c_3 + LAI_{d-1}, \text{ leaf} - \text{off}, t_d < 12 \, h \end{cases} \quad (19)$$

11   where GDD and SDD are the growing and senescence degree days, $b_{1,2,3}$ and $c_{1,2,3}$ control the

12   rate of change in LAI and $T_{BaseSDD}$ is the base temperature for senescence. Using the original

13   LAI functions with coefficients $b_1 = b_2 = 0.03$ and $c_1 = c_2 = 5 \cdot 10^{-4}$ resulted too slow both leaf-

14   on and leaf-off period at both cities when compared to visual inspection. Thus, for the leaf-on

15   period the coefficients at both cities were changed to $b_1 = 0.04$ and $c_1 = 0.001$, and the new

16   senescence parameterization (Eq. 20) based on the day length with parameters $b_3 = -1.5$ and

17   $c_3 = 1.5 \cdot 10^{-3}$ was deployed. Unfortunately no measurements of LAI were available. The

18   values are from visual surveys of leaf-on and leaf-off timings.

19

20

21

22

23

24

25

26

27

28

1    Appendix B. Snow fraction depletion curves for vegetated, paved and roof surfaces.
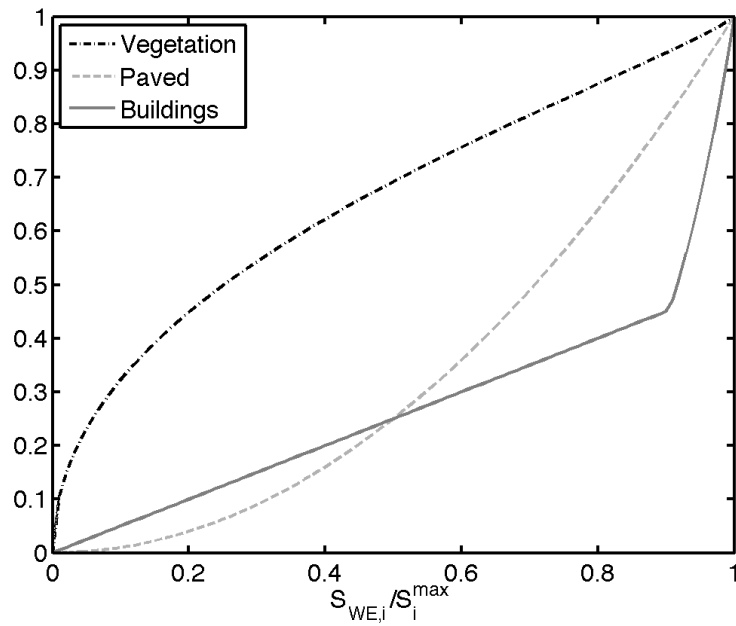


2

3    Figure B01. Surface snow fraction depletion curves for vegetated, paved and building

4    surfaces. The paved and building curves was obtained from Valeo and Ho (2004), whereas

5    the vegetation curve was obtained by fitting Swenson and Lawrence (2012) to Ek et al.

6    (2003) data.

7

8

9

10

11

12

13

14

15

16

17

18

1    Appendix C. Notation used

2    $\alpha_i$                 Effective surface albedo (-)

3    $\alpha_s$                 Effective snow albedo (-)

4    $\alpha_s^{min}$           Minimum snow albedo (-)

5    $\alpha_s^{max}$           Minimum snow albedo (-)

6    $\Delta Q^*$               Change in the net-all wave radiation in time step $\Delta t$ (W m$^{-2}$)

7    $\Delta Q_A$               Advective heat flux (W m$^{-2}$)

8    $\Delta Q_{S,I}$           Change in the snow heat storage (W m$^{-2}$)

9    $\Delta S_{WE}$            Change in the snow water equivalent (mm h$^{-1}$)

10   $\Delta t$                 Time step of the model (s)

11   $\varepsilon_i$            Effective surface emissivity (-)

12   $\varepsilon_s$            Effective surface emissivity of snow (-)

13   $\gamma$                   Psychometric constant (Pa °C$^{-1}$)

14   $\lambda_{bldg}$           Surface fraction of buildings (-)

15   $\lambda_{dec}$            Surface fraction of deciduous trees (-)

16   $\lambda_{ev}$             Surface fraction of evergreens (-)

17   $\lambda_{grass}$          Surface fraction of non-irrigated grass (-)

18   $\lambda_{igrass}$         Surface fraction of grass (-)

19   $\lambda_{pav}$            Surface fraction of paved areas (-)

20   $\lambda_{unman}$          Surface fraction of unmanaged land (-)

21   $\lambda_{veg}$            Surface fraction of vegetation  (-)

22   $\lambda_{water}$          Surface fraction of water (-)

23   $\rho$                     Air density (kg m$^{-3}$)

24   $\rho_e$                   Threshold value in the calculation of retention capacity (kg m$^{-3}$)

25   $\rho_s$                   Snow density (kg m$^{-3}$)

26   $\rho_{s,0}$               Initial snow density (kg m$^{-3}$)

27   $\rho_w$                   Water density (kg m$^{-3}$)

28   $\rho_s^{max}$             Maximum snow density (kg m$^{-3}$)

29   $\rho_s^{min}$             Minimum snow density (kg m$^{-3}$)

30   $\tau_a$                   Cold snow time constant for snow albedo aging (-)

31   $\sigma_{Obs}$             Standard deviation of observed values

32   $\tau_d$                   Seconds in one hour (3600 s h$^{-1}$)

33   $\tau_h$                   Period of one day (86400 s)

34   $\tau_f$                   Warm snow time constant for snow albedo aging (-)

| 1 | $\tau_r$ | Time constant describing the snow density aging (-) |
|---|---|---|
| 2 | $a_{0,\{wd,we\}}$ | Parameter defining the base $Q_f$ per capita (W m$^{-2}$ (capita$^{-1}$ ha$^{-1}$)$^{-1}$) |
| 3 | $a_{1,\{wd,we\}}$ | Parameter related to CDD (W m$^{-2}$ K$^{-1}$ (capita$^{-1}$ ha$^{-1}$)$^{-1}$) |
| 4 | $a_{2,\{wd,we\}}$ | Parameter related to HDD (W m$^{-2}$ K$^{-1}$ (capita$^{-1}$ ha$^{-1}$)$^{-1}$) |
| 5 | $a_{1,2,3}$ | Constants in the calculation of the snow heat storage |
| 6 | $a_r$ | Radiation melt factor (mm W$^{-1}$ h$^{-1}$) |
| 7 | $a_t$ | Temperature melt factor (mm °C$^{-1}$ h$^{-1}$) |
| 8 | $a_f$ | Temperature freezing factor (mm °C$^{-1}$ h$^{-1}$) |
| 9 | $A$ | Study area (ha) |
| 10 | $b$ | Empirical coefficient in the calculation of drainage |
| 11 | $b_{1,2,3}$ | Parameters controlling the speed of leaf on |
| 12 | $b_{1a,2a,3a}$ | Parameters for automatic irrigation (mm, mm K$^{-1}$, mm d$^{-1}$) |
| 13 | $b_{1m,2m,3m}$ | Parameters for manual irrigation (mm, mm K$^{-1}$, mm d$^{-1}$) |
| 14 | Bldg | Building surface type |
| 15 | $c_{1,2,3}$ | Parameter to control the speed of leaf-off |
| 16 | $c_p$ | Heat capacity of air (J kg$^{-1}$ K$^{-1}$) |
| 17 | $c_w$ | Specific heat capacity of water (kJ kg$^{-1}$ °C$^{-1}$) |
| 18 | $C_i$ | Interception state of ith surface (mm) |
| 19 | $C_{soil,i}$ | Soil water storage (mm) |
| 20 | $C^R$ | Retention capacity (mm) |
| 21 | $C^R_{min}$ | Minimum retention capacity (mm) |
| 22 | $C^R_{max}$ | Maximum retention capacity (mm) |
| 23 | $d$ | Day |
| 24 | $D_{0,i}$ | Drainage rate (mm) |
| 25 | $D_{sm}$ | Day of the snow melt |
| 26 | Decid | Deciduous surface type |
| 27 | $E$ | Evaporation (mm h$^{-1}$) |
| 28 | EC | Eddy covariance |
| 29 | Everg | Evergreen surface type |
| 30 | $f_{s,i}$ | Fraction of snow on surface |
| 31 | $f_{s,i,0}$ | Initial fraction of snow |
| 32 | $F$ | Freezing water on surface (mm h$^{-1}$) |
| 33 | $g_{i,max}$ | Maximum conductance (m s$^{-1}$) |
| 34 | $G_{1-6}$ | Parameters related to surface conductance |
| 35 | GDD | Growing degree days |

| 1 | $i$ | Surface type index |
|---|---|---|
| 2 | Irr. veg. | Irrigated vegetation type |
| 3 | $I$ | Interception of linear regression |
| 4 | $I_w$ | Additional water to water surface type (mm) |
| 5 | $K{\downarrow}$ | Downward shortwave radiation (W m$^{-2}$) |
| 6 | $K{\downarrow}_m$ | Maximum incoming solar radiation used in $g_s$ calculation |
| 7 | $K{\uparrow}$ | Upward shortwave radiation (W m$^{-2}$) |
| 8 | $K_s$ | Saturated hydraulic conductivity (mm s$^{-1}$) |
| 9 | Ku | Kumpula site |
| 10 | Ku1 | Built sector at the Kumpula site |
| 11 | Ku2 | Road sector at the Kumpula site |
| 12 | Ku3 | Vegetation sector at the Kumpula site |
| 13 | $L_f$ | Latent heat of fusion (J kg$^{-1}$) |
| 14 | $LAI_{d,i}$ | Daily leaf area index (m$^2$ m$^{-2}$) |
| 15 | $LAI_{max,i}$ | Maximum LAI of surface type $i$ (m$^2$ m$^{-2}$) |
| 16 | $LAI_{min,i}$ | Maximum LAI of surface type $i$ (m$^2$ m$^{-2}$) |
| 17 | Lat | Latitude (°) |
| 18 | Lon | Longitude (°) |
| 19 | $M$ | Snow melt and re-freezing of melted water (mm h$^{-1}$) |
| 20 | MBE | Mean biased error |
| 21 | nRMSE | Normalized root mean square error |
| 22 | $N$ | Number of data points |
| 23 | OHM | Objective hysteresis model |
| 24 | $p$ | Population density inside the grid (capita ha$^{-1}$) |
| 25 | $P$ | Precipitation (mm h$^{-1}$) |
| 26 | Pa | Pasila site |
| 27 | Pav | Paved surface type |
| 28 | Pi | Pihlajamäki site |
| 29 | Pr | Pierrefonds-Roxboro site |
| 30 | $Q*$ | Net all-wave radiation (W m$^{-2}$) |
| 31 | $Q_A$ | Advective heat flux (W m$^{-2}$) |
| 32 | $Q_E$ | Latent heat flux (W m$^{-2}$) |
| 33 | $Q_f$ | Anthropogenic heat flux (W m$^{-2}$) |
| 34 | $Q_g$ | Ground heat flux (W m$^{-2}$) |
| 35 | $Q_H$ | Sensible heat flux (W m$^{-2}$) |

| 1 | $Q_M$ | Energy consumed to melt snow (W m$^{-2}$) |
|---|---|---|
| 2 | $Q_p$ | Heat released from rain on snow (W m$^{-2}$) |
| 3 | $r$ | Pearsons correlation coefficient |
| 4 | $r_a$ | Aerodynamic resistance (s m$^{-1}$) |
| 5 | $r_{s,max}$ | Maximum surface resistance (s m$^{-1}$) |
| 6 | $res_{cap}$ | Surface water capacity in LUMPS (mm) |
| 7 | $res_{drain}$ | Drainage rate of water bucket in LUMPS (mm h$^{-1}$) |
| 8 | $R$ | Runoff (mm) |
| 9 | $R_C$ | Limit when surface is totally covered with water in LUMPS (mm) |
| 10 | Rl | Rosemont-La-Petite-Patrie site |
| 11 | $R_{mod}$ | Modelled runoff (mm) |
| 12 | $R_{obs}$ | Observed runoff (mm) |
| 13 | RMSE | Root mean square error |
| 14 | $s$ | Slope of the saturation vapour pressure curve over ice (Pa °C$^{-1}$) |
| 15 | $s_d$ | Snow depth (m) |
| 16 | sRMSE | RMSE normalized with standard deviation of the observation |
| 17 | $S$ | Slope of linear regression |
| 18 | $S_{1-2}$ | Parameters related to surface conductance |
| 19 | $S_i$ | State of the snow-free surface (mm) |
| 20 | $S_{Pipe}$ | Maximum depth capacity of pipes (mm) |
| 21 | $S_{soil,i}$ | Soil state (mm) |
| 22 | $S_{WE}$ | Snow water equivalent (mm) |
| 23 | $S_{WE,0}$ | Initial snow water equivalent (mm) |
| 24 | $S_{WE,Lim}$ | Limit of the snow water equivalent for the snow removal (mm) |
| 25 | $S_{WE,i}^{max}$ | Snow water equivalent when surface type $i$ is fully covered with snow (mm) |
| 26 | SDD | Senescence degree days |
| 27 | SUEWS | the Surface Urban Energy and Water balance Scheme |
| 28 | $t_d$ | Day length (h) |
| 29 | $T_a$ | Air temperature (°C) |
| 30 | $T_{BaseGDD}$ | Base temperature for leaf growth (°C) |
| 31 | $T_{BaseSDD}$ | Base temperature for senescence (°C) |
| 32 | $T_{BaseQF}$ | Base temperature for $Q_F$ (°C) |
| 33 | $T_H, T_L$ | Parameters related to calculation of $g_s$ (°C) |
| 34 | $T_{lim}$ | Temperature limit for the liquid precipitation and snow (°C) |
| 35 | $T_s$ | Snow surface temperature (°C) |

| 1 | $T_{Step}$ | Time step for water balance calculation(s) |
| 2 | $T_R$ | Transport of snow from the study area (mm) |
| 3 | $V$ | Vapour pressure deficit (Pa) |
| 4 | $X_{Mod}$ | Modelled variable $X$ |
| 5 | $X_{Mod,\ max}$ | Maximum value of observed time series |
| 6 | $X_{Obs}$ | Observed variable $X$ |
| 7 | $X_{Obs,\ max}$ | Maximum value of observed time series |
| 8 | $z$ | Height of the meteorological measurements (m) |
| 9 | $z_{0v}$ | Roughness length for heat and water vapour (m) |
| 10 | $z_{0m}$ | Roughness length for momentum (m) |
| 11 | $z_h$ | Mean building height (m) |
| 12 | $z_t$ | Mean tree height (m) |
| 13 | | |
| 14 | | |
| 15 | | |
| 16 | | |
| 17 | | |
| 18 | | |
| 19 | | |
| 20 | | |
| 21 | | |
| 22 | | |
| 23 | | |
| 24 | | |
| 25 | | |
| 26 | | |
| 27 | | |
| 28 | | |
| 29 | | |